

1. EXPLANATORY NOTES¹

Shipboard Scientific Party²

In this chapter, we have assembled information that will help the reader understand the basis for our preliminary conclusions and also help the interested investigator select samples for further analysis. This information concerns only shipboard operations and analyses described in the site chapters in the *Initial Reports* volume of the Leg 129 *Proceedings of the Ocean Drilling Program*. Methods used by various investigators for shore-based analysis of Leg 129 data will be detailed in the individual scientific contributions published in the *Scientific Results* volume.

AUTHORSHIP OF SITE CHAPTERS

The separate sections of the site chapters were written by the following shipboard scientists (authors are listed in alphabetical order, no seniority is necessarily implied):

Site Summary (Lancelot, Larson)
Background and Objectives (Lancelot, Larson)
Operations (Lancelot, Larson)
Sedimentology and Lithostratigraphy (Behl, Karl, Karpoff, Ogg, Salimulah)
Biostratigraphy (Covington, Durr, Erba, Hauser, Mat-suoka, Wightman)
Paleomagnetism (Steiner, Wallick)
Inorganic Geochemistry (France-Lanord)
Igneous Petrology (Castillo, Floyd, France-Lanord)
Physical Properties (Busch, Cameron)
Downhole Measurements (Abrams, Fisher, Molinie)
Site Geophysics and Seismic Stratigraphy (Abrams, Lancelot, Larson)
Conclusions (Lancelot, Larson)
Appendix (Shipboard Scientific Party)

Following the text of each site chapter are summary downhole logs. Core descriptions ("barrel sheets" and igneous rock visual core descriptions) and photographs of each core appear in Section 3, near the back of this volume.

DEFINITIONS

Conventional Use of Time and Time-Rock Units

The subdivisions of epochs/series into *early*, *middle*, *late*, or *lower*, *middle*, *upper* have no real formal standing in stratigraphy. The subdivision of lithostratigraphic (rock), chronostratigraphic (time-rock), and geochronologic (time) units is defined as follows throughout this volume.

Lithostratigraphic Units

For rock units, the terms *lower*, *middle*, and *upper* describe sections of rocks subdivided on the basis of superposition, without any implication of time-partitioning.

Chronostratigraphic Units

These units imply bodies of strata formed during specific intervals of geologic time. According to convention they are subdivided using the terms *lower*, *middle*, and *upper*. The basis of formal time-rock units are stages, each of which has (or should have) a stratotype, a standard section with which other sections can be compared. Stages are conventionally grouped together into the subunits that subdivide the series. When referring to the entire subdivision of the series, the terms Lower, Middle, and Upper are capitalized by convention. The lowercase forms, lower, middle, and upper, refer only to a portion of the subunit or its equivalent, or instead imply informal usage.

Geochronologic Units

When speaking of time, age, or of sections in the temporal sense, the terms *early*, *middle*, and *late* are used for subdivision. The basis of the formal geochronologic units are ages (time equivalent of stages). Like stages, ages grouped together form the time subunits that subdivide epochs. When referring to the entire subunit, the terms Early, Middle, and Late are capitalized, but not when only a part of the subunit, or an informal sense is implied. However, such combinations as early Early, middle Early, late Early, etc., are used to refer to older, medial, or younger parts of the entire subunit.

Use of Ma vs. m.y.

Ma is equivalent to and replaces m.y.B.P. (million years Before Present), e.g., 35–40 Ma. The abbreviation *m.y.* is still used in sentences such as, "...for five m.y. in the early Miocene."

DRILLING CHARACTERISTICS

Information concerning sedimentary stratification in uncovered or unrecovered intervals may be inferred from seismic data, wireline-logging results, and from an examination of the behavior of the drill string as observed and recorded on the drilling platform. Typically, the harder a layer, the slower and more difficult it is to penetrate. A number of other factors may determine the rate of penetration, so it is not always possible to relate the drilling time directly to the hardness of the layers. Bit weight and revolutions per minute, recorded on the drilling recorder, also influence the penetration rate.

DRILLING DEFORMATION

When cores are split, many show signs of significant sediment disturbance, including the concave-downward appearance of originally horizontal bands, haphazard mixing of lumps of different lithologies (mainly at the tops of cores), and the near-fluid state of some sediments recovered from tens to hundreds of meters below the seafloor. Core deformation probably occurs during cutting, retrieval (with accompanying changes in pressure and temperature), and core handling on

¹ Lancelot, Y., Larson, R. L., et al., 1990. *Proc. ODP, Init. Repts.*, 129: College Station, TX (Ocean Drilling Program).

² Shipboard Scientific Party is as given in the list of participants preceding the contents.

deck. A detailed discussion of slump-like drilling disturbance is given in the "Core Description" section of this chapter.

SHIPBOARD SCIENTIFIC PROCEDURES

Numbering of Sites, Holes, Cores, and Samples

Ocean Drilling Program (ODP) drill sites are numbered consecutively and refer to one or more holes drilled while the ship was positioned over one acoustic beacon. Multiple holes may be drilled at a single site by pulling the drill pipe above the seafloor (out of the hole), moving the ship some distance from the previous hole, and then drilling another hole.

For all ODP drill sites, a letter suffix distinguishes each hole drilled at the same site. For example, the first hole drilled is assigned the site number modified by the suffix A, the second hole takes the site number and suffix B, and so forth. Note that this procedure differs slightly from that used by the Deep Sea Drilling Project (DSDP) (Sites 1 through 624), but prevents ambiguity between site- and hole-number designations. It is important to distinguish among holes drilled at a site, because recovered sediments or rocks from different holes usually do not come from equivalent positions in the stratigraphic column.

The cored interval is measured in meters below seafloor (mbsf). The depth interval assigned to an individual core begins with the depth below the seafloor that the coring operation began, and extends to the depth that the coring operation ended (see Fig. 1). For example, each coring interval is generally up to 9.5 m long, which is the length of a core barrel. Coring intervals may be shorter and may not necessarily be adjacent if separated by drilled intervals. In soft sediments, the drill string can be "washed ahead" with the core barrel in place, without recovering sediments. This is achieved by pumping water down the pipe at high pressure to wash the sediment out of the way of the bit and up the space between the drill pipe and the wall of the hole. If thin, hard, rock layers are present, then it is possible to get "spotty" sampling of these resistant layers within the washed interval, and thus to have a cored interval greater than 9.5 m. In drilling hard rock, a center bit may replace the core barrel if it is necessary to drill without core recovery.

Cores taken from a hole are numbered serially from the top of the hole downward. Core numbers and their associated cored intervals (in mbsf) usually are unique in a given hole. This may not be true, however, if an interval must be cored twice because of caving of cuttings or other hole problems. Maximum full recovery for a single core is 9.5 m of rock or sediment contained in a plastic liner (6.6-cm internal diameter) plus about 0.2 m (without a plastic liner) in the core catcher (Fig. 2). The core catcher is a device at the bottom of the core barrel which prevents the core from sliding out when the barrel is being retrieved from the hole. In certain situations (e.g., when coring gas-charged sediments that expand while being brought on deck) recovery may exceed the 9.5-m maximum.

A recovered core is divided into 1.5-m sections that are numbered serially from the top (Fig. 2). When full recovery is obtained, the sections are numbered from 1 through 7, with the last section possibly being shorter than 1.5 m (rarely, an unusually long core may require more than 7 sections). When less than full recovery is obtained, there will be as many sections as needed to accommodate the length of the core recovered. For example, 4 m of core would be divided into two 1.5-m sections and one 1-m section. If cores are fragmented (recovery less than 100%), sections are numbered serially and intervening sections are noted as void, whether shipboard scientists believe that the fragments were contigu-

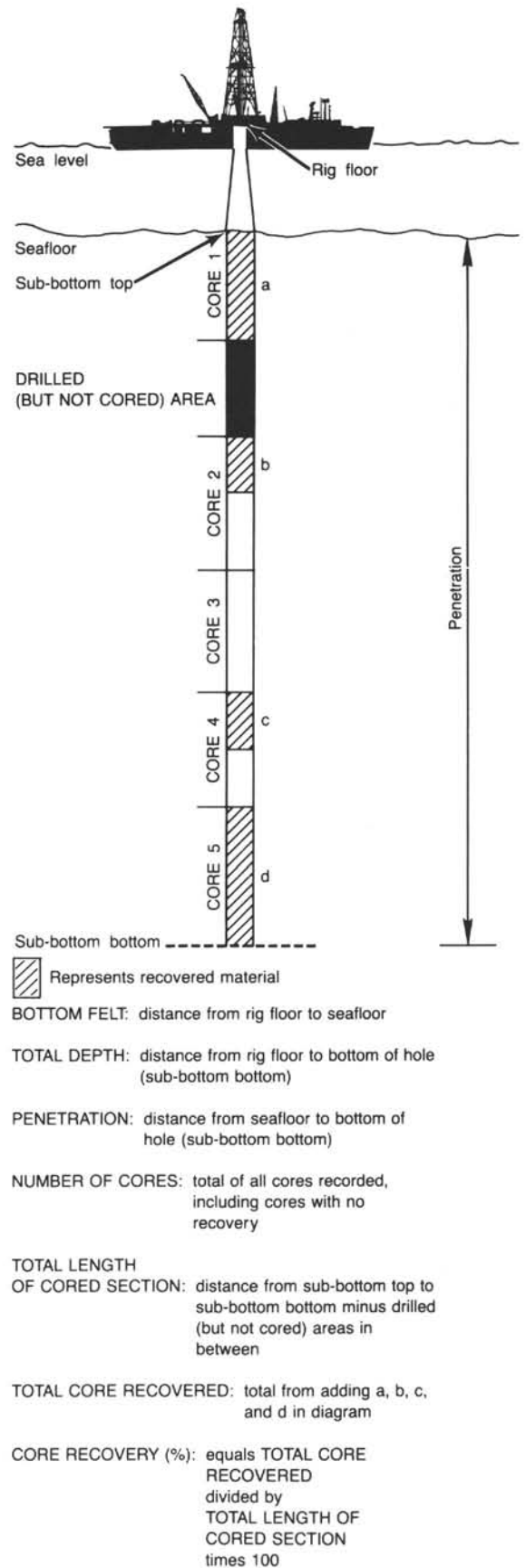


Figure 1. Coring and depth intervals.

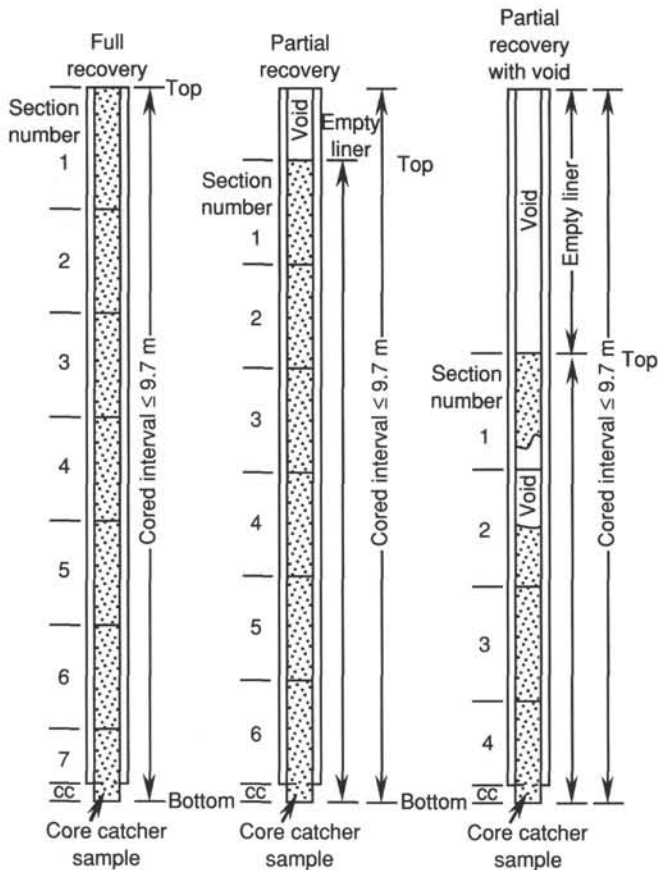


Figure 2. Examples of numbered core sections.

ous *in situ* or not. In rare cases, a section less than 1.5 m may be cut in order to preserve features of interest (e.g., lithologic contacts).

By convention, material recovered from the core catcher is placed below the last section when the core is described, and labeled core catcher (CC); in sedimentary cores, it is treated as a separate section. The core catcher is placed at the top of the cored interval in cases where material is only recovered in the core catcher. However, information supplied by the drillers or by other sources may allow for more precise interpretation as to the correct position of core catcher material within an incompletely recovered cored interval.

Igneous rock cores are also cut into 1.5-m sections that are numbered serially; each piece of rock is then assigned a number. Fragments of a single piece are assigned a single number, and individual fragments are identified alphabetically. The core-catcher sample is placed at the bottom of the last section and is treated as part of the last section rather than as a separate piece. Scientists completing visual core descriptions describe each lithologic unit, noting core and section boundaries only as physical reference points.

When, as is usually the case, the recovered core is shorter than the cored interval, the top of the core is equated with the top of the cored interval by convention, in order to achieve consistency in handling analytical data derived from the cores. Samples removed from the cores are designated by distance measured in centimeters from the top of the section to the top and bottom of each sample removed from that section. In curated hard-rock sections, sturdy plastic spacers are placed between pieces that do not fit together in order to protect them

from damage in transit and in storage. Therefore, the centimeter interval noted for a hard-rock sample has no direct relationship to that sample's depth within the cored interval, but is only a physical reference to the location of the sample within the curated core.

A full identification number for a sample consists of the following information: leg, site, hole, core number, core type, section number, piece number (for hard rock), and interval in centimeters measured from the top of section. For example, a sample identification of "129-800A-25R-1, 10-12 cm" represents a sample removed from the interval between 10 and 12 cm below the top of Section 1, Core 25 (R designates that this core was taken during rotary drilling) of Hole 800A during Leg 129.

All ODP core and sample identifiers indicate core type. The following abbreviations are used: R = rotary core barrel (RCB); H = hydraulic piston core (HPC; also referred to as APC, or advanced hydraulic piston core); P = pressure core barrel; X = extended core barrel (XCB); B = drill-bit recovery; C = center-bit recovery; I = *in-situ* water sample; S = sidewall sample; W = wash-core recovery; and M = miscellaneous material. On Leg 129, only RCB cores were recovered.

Core Handling

Sediments

As soon as a core is retrieved on deck, a sample is taken from the core catcher and given to the paleontological laboratory for an initial age assessment. The core is then placed on the long horizontal rack, and gas samples may be taken by piercing the core liner and withdrawing gas into a vacuum tube. Voids within the core are sought as sites for gas sampling. Some of the gas samples are stored for shore-based study, but others are analyzed immediately as part of the shipboard safety and pollution prevention program. Next, the core is marked into section lengths, each section is labeled, and the core is cut into sections. Interstitial-water (IW), organic geochemistry (OG), and physical properties (PP) samples are then taken. In addition, some headspace gas samples (HS) are scraped from the ends of cut sections on the catwalk and sealed in glass vials for light hydrocarbon analysis. Each section is then sealed at the top and bottom by gluing on color-coded plastic caps: blue to identify the top of a section and clear for the bottom. A yellow cap is placed on the section ends from which a whole-round sample has been removed. The caps are usually attached to the liner by coating the end liner and the inside rim of the cap with acetone, and then the caps are taped to the liners.

The cores are then carried into the laboratory, where the sections are again labeled using an engraver to permanently mark the full designation of the section. The length of the core in each section and the core-catcher sample are measured to the nearest centimeter, and this information is logged into the shipboard core-log database program.

Whole-round sections from APC and XCB cores are normally run through the multisensor track (MST). The MST includes the GRAPE (gamma-ray attenuation porosity evaluator) and *P*-wave logger devices, which measure bulk density, porosity, and sonic velocity, and also includes a meter which determines the volume magnetic susceptibility. As all material collected during Leg 129 was rotary-cored, the sediments were far too disturbed for testing with the standard MST. Individual samples removed from split cores were subjected to a 2-min GRAPE count, as described in the "Physical Properties" section (this chapter). After the core has equilibrated to room temperature (approximately 3 hr), thermal conductivity measurements are performed on relatively soft sediments, and the cores are split.

Cores of soft material are split lengthwise into *working* and *archive* halves. The softer cores are split with a wire or saw, depending on the degree of induration. Harder cores are split with a band saw or diamond saw. The wire-cut cores are split from the bottom to top, so investigators should be aware that older material could have been transported up the core on the split face of each section.

The working half of the core is sampled for both shipboard and shore-based laboratory studies. Each extracted sample is logged into the sampling computer database program by the location and the name of the investigator receiving the sample. Records of all removed samples are kept by the curator at ODP headquarters. The extracted samples are sealed in plastic vials or bags and labeled. Samples are routinely taken for shipboard physical properties analysis and subsequently used for determining calcium carbonate (CaCO_3) (coulometric analysis) and organic carbon (CNS elemental analyzer,) and the data are reported in the site chapters.

The archive half is described visually. Smear slides are made from samples taken from the archive half, and are supplemented by thin sections and X-ray-diffraction (XRD) samples taken from the working half. Most archive sections are run through the cryogenic magnetometer. The archive half is then photographed with both black-and-white and color film, a whole core at a time. Close-up photographs (black-and-white) are taken of particular features for illustrations in the summary of each site, as requested by scientists.

Both halves of the core are then put into labeled plastic tubes, sealed, and transferred to cold-storage space aboard the drilling vessel. At the end of the leg, the cores are transferred from the ship in refrigerated airfreight containers to cold storage at the Gulf Coast Repository at the Ocean Drilling Program, Texas A&M University, College Station, Texas.

Igneous and Metamorphic Rocks

Igneous and metamorphic rock cores are handled differently from sedimentary cores. Once on deck, the core catcher is placed at the bottom of the core liner and total core recovery is calculated by shunting the rock pieces together and measuring to the nearest centimeter. The core is then cut into 1.5-m-long sections and transferred to the lab.

The contents of each section are transferred into 1.5-m-long sections of split core liner, where the bottom of oriented pieces (i.e., pieces that clearly could not have rotated top to bottom about a horizontal axis in the liner) are marked with a red wax pencil. This is to ensure that orientation is not lost during the splitting and labeling process. The core is then split into archive and working halves. A plastic spacer is used to separate individual pieces and/or reconstructed groups of pieces in the core liner. These spacers may represent a substantial interval of no recovery. Each piece is numbered sequentially from the top of each section, beginning with number 1; reconstructed groups of pieces are assigned the same number, but are lettered consecutively. Pieces are labeled only on external surfaces. If the piece is oriented, an arrow is added to the label pointing to the top of the section.

The working half of the hard-rock core is then sampled for shipboard laboratory studies. Records of all samples are kept by the curator at ODP headquarters. Minicore samples are routinely taken for physical properties and magnetic studies. Some of these samples are later subdivided for thin-sectioning, so that as many measurements as possible are made on the same pieces of rock. At least one minicore is taken per lithological unit when recovery permits, generally from the freshest areas of core. Additional thin sections and XRD samples are selected from areas of particular interest. Samples

for shore-based studies are selected in a sampling party held after drilling has ended.

The archive half is described visually, then photographed with both black-and-white and color film, one core at a time. Both halves of the core are then shrink-wrapped in plastic to prevent rock pieces from vibrating out of sequence during transit, put into labeled plastic tubes, sealed, and transferred to cold-storage space aboard the drilling vessel.

VISUAL CORE DESCRIPTION

Sediment "Barrel Sheets"

The core description forms (Fig. 3), or "barrel sheets," summarize the data obtained during shipboard analysis of each sediment core. The following discussion explains the ODP conventions used in compiling each part of the core-description forms and the exceptions to these procedures adopted by the Leg 129 scientific party.

Sediments and Volcaniclastic Deposits

Shipboard sedimentologists were responsible for visual core logging, smear slide analyses, and thin-section descriptions of sedimentary and volcaniclastic material. Mineral composition data, determined by X-ray diffraction, were used to augment the visual core descriptions. Data on biostratigraphy (age), geochemistry (CaCO_3 , C_{org}), magnetics, and physical properties (wet-bulk density and porosity), were integrated with the sedimentological information.

Core Designation

Cores are designated using leg, site, hole, core number, and core type as discussed in a preceding section (see "Numbering of Sites, Holes, Cores, and Samples" section, this chapter). The cored interval is specified in terms of meters below sea level (mbsl) and meters below seafloor (mbsf). On the basis of drill-pipe measurements (DPM), reported by the SEDCO coring technician and the ODP operations superintendent, depths are corrected for the height of the rig floor dual elevator stool above sea level to give true water depth and correct mbsl.

Graphic Lithology Column

The lithology of the material recovered is represented on the core description forms, by a single symbol or by two or more symbols (see Fig. 4). Where an interval of sediment or sedimentary rock is a mixture, the constituent categories are separated by a solid vertical line, with each category represented by its own symbol. In an interval composed of two or more sediment types that have quite different composition, such as thin-bedded and highly variegated sediments, the average relative abundances of the constituents are represented graphically by dashed lines that vertically divide the interval into appropriate fractions as described above.

The graphic lithology column only shows the composition of layers or intervals exceeding 10 cm in thickness. Information on finer-scale lithologic variations is included in the VCD (visual core description) forms available from ODP upon request.

Where sedimentary material was intercalated with igneous rocks, the igneous petrologists described the igneous section and recorded results under "Hard Rock Core Description Forms." These are referred to on the sedimentary barrel sheets as "see igneous rock description."

Sedimentary Structures

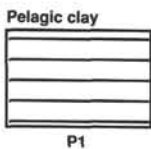
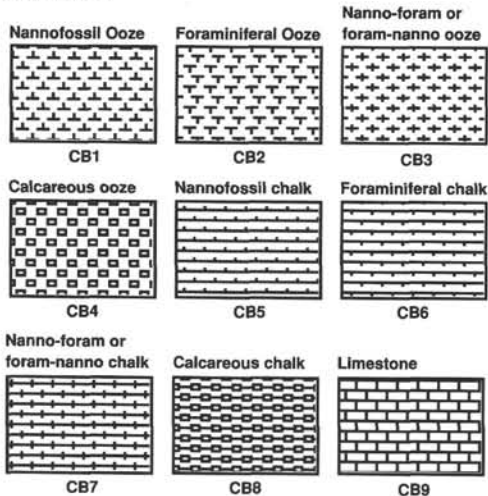
In sediment cores, natural structures and structures created by the coring process can be difficult to distinguish. Natural structures observed are indicated in the "Sedimenta-

SITE		HOLE				CORE		CORED INTERVAL					
TIME-ROCK UNIT	BIOSTRAT. ZONE/ FOSSIL CHARACTER				PALEOMAGNETICS	PHYS. PROPERTIES	CHEMISTRY	SECTION	METERS	GRAPHIC LITHOLOGY	DRILLING DISTURB. SED. STRUCTURES	SAMPLES	LITHOLOGIC DESCRIPTION
	FORAMINIFERS	NANNOFOSSILS	RADIOLARIANS	DIATOMS									
								0.5 1 1.0					
								2					
								3				OG ← Organic geochemistry sample	
								4					Smear slide and thin section summary (%) Section, depth (cm) M = minor lithology D = dominant lithology
								5				IW ← Interstitial water sample	
								6				* ← Smear slide # ← Thin section	
								7					
								CC					

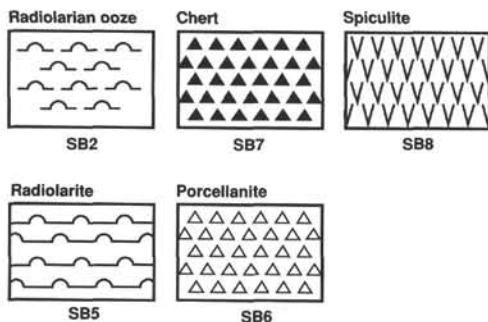
Figure 3. Core description form ("barrel sheet") used for sediments and sedimentary rocks.

PELAGIC SEDIMENTS

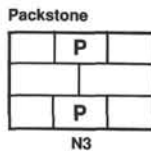
Calcareous



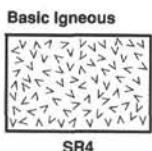
Siliceous



NERITIC SEDIMENTS



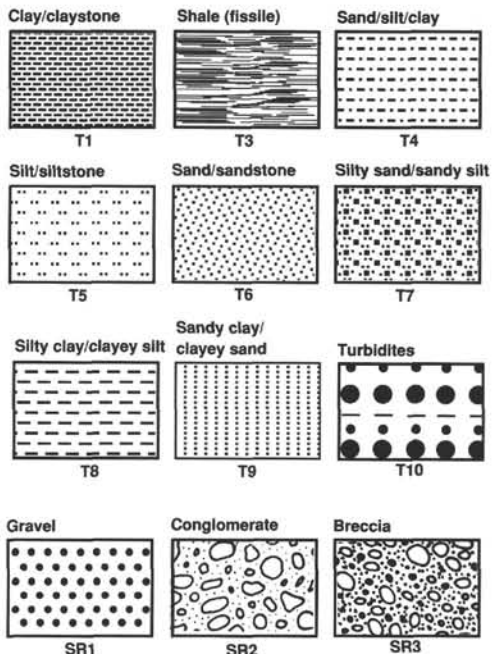
SPECIAL ROCK TYPES



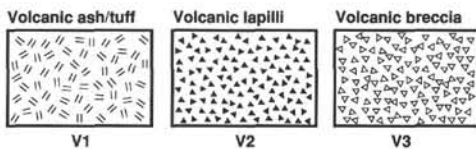
CHEMICAL SEDIMENTS



Drawn circle with symbol (others may be designated)



VOLCANICLASTIC SEDIMENTS



MIXED SEDIMENTS

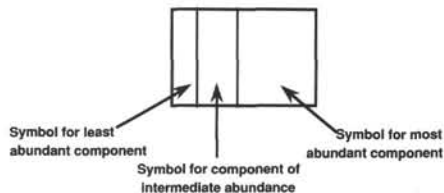


Figure 4. Key to symbols used in the "graphic lithology" column on the core description form shown in Figure 3.

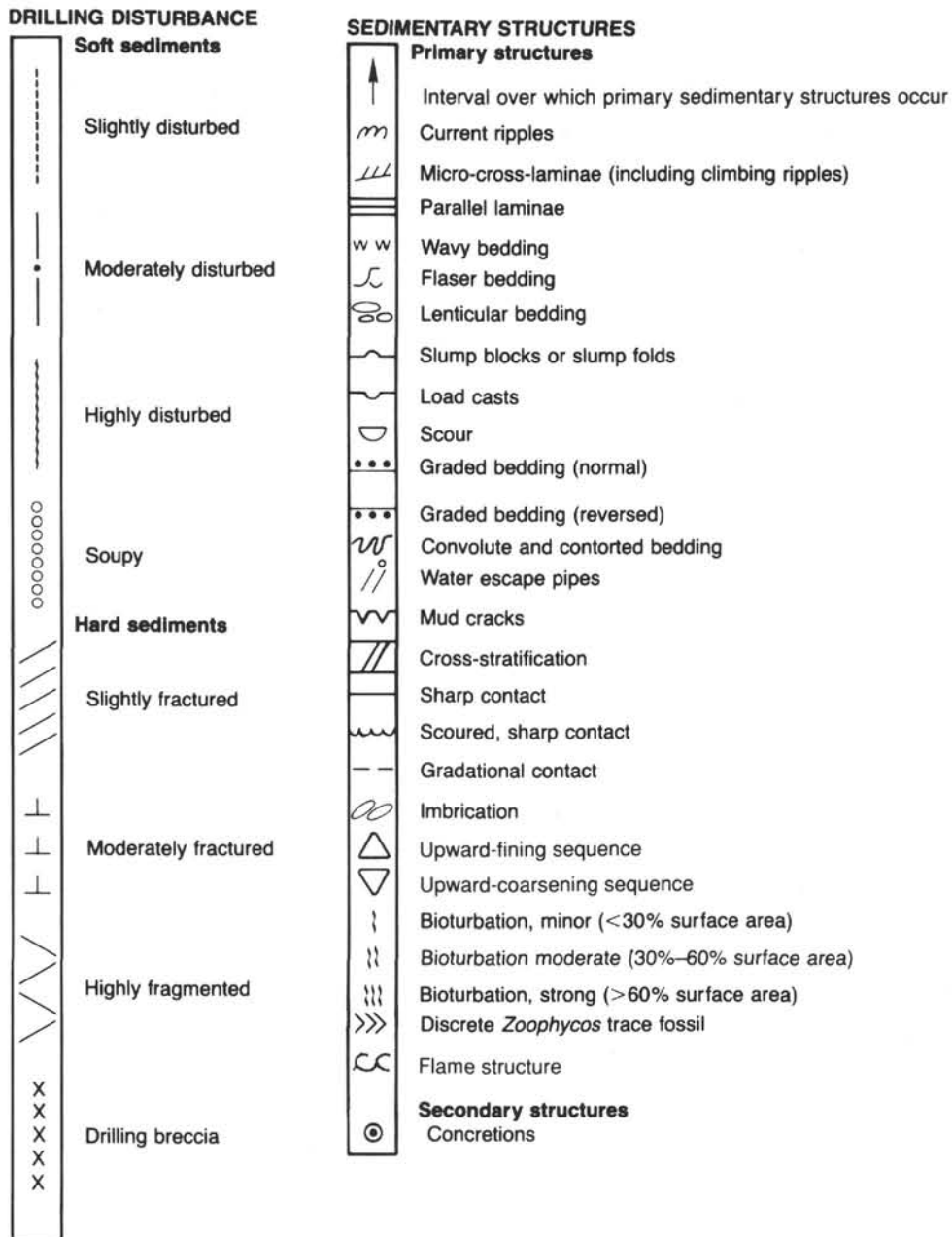


Figure 5. Symbols used for drilling disturbance and sedimentary structures on core description forms shown in Figure 3.

ry Structure” column of the core description form. The symbols used to describe the primary biogenic and physical sedimentary structures, and secondary structures such as microfaults, dewatering veinlets, and mineral-filled fractures, are given in Figure 5. Two new symbols were added to the usual key. A wavy line indicates the presence of flame structures, which are common in turbidites. Triangles with different heights represent turbidite beds fining upwards.

Sediment Disturbance

This is illustrated in the “Drilling Disturbance” column on the core description form (using the symbols in Fig. 5). Blank regions indicate a lack of drilling disturbance. Drilling distur-

bance is recognized for soft and firm sediments using these categories:

1. Slightly deformed: Bedding contacts are slightly bent.
2. Moderately deformed: Bedding contacts have undergone extreme bowing.
3. Highly deformed: Bedding is completely disturbed, sometimes showing symmetrical diapir-like or flow structures.
4. Soupy: Intervals are water-saturated and have lost all aspects of original bedding.

The degree of fracturing in indurated sediments and igneous rocks is described using the following categories:

1. Slightly fractured: Core pieces are in place and contain little drilling slurry or breccia;
2. Moderately fragmented: Core pieces are in place or partly displaced, but original orientation is preserved or recognizable (drilling slurry may surround fragments);
3. Highly fragmented: Pieces are from the interval cored and probably in correct stratigraphic sequence (although they may not represent the entire section), but original orientation is completely lost;
4. Drilling breccia: Core pieces have lost their original orientation and stratigraphic position and may be mixed with drilling slurry.

Induration

The criteria used to determine the induration of pelagic sediments found during Leg 129 are those of Gealy et al. (1971). These criteria are subjective and provide three classes for pelagic oozes:

1. Soft: Sediments that have little strength and are readily deformed under the finger or broad blade of the spatula are termed oozes or clay.
2. Firm: Partly lithified pelagic sediments as oozes or clays are readily deformed under the fingernail of the edge of a spatula blade.
3. Hard: Nonfriable, cemented rocks.

The suffix "-stone" is added to the name of cemented rocks (e.g., limestone, claystone). Hard siliceous sedimentary rocks are called chert or porcellanite (see "Sediment Classification" section, this chapter).

Color

Colors were determined by comparison with Munsell soil-color charts. Colors were determined immediately after the cores were split because redox-associated color changes may occur when deep-sea sediments are exposed to the atmosphere. Information on core colors is given in the text of the "Lithologic Description" on the core description forms.

Samples

The position of samples taken from each core for shipboard analysis is indicated in the "Samples" column on the core description form (Fig. 3). The symbol "*" indicates the location of smear slide samples, and the symbol "#" indicates the location of thin-section samples. The notations IW and OG designate the location of samples for whole-round interstitial water geochemistry and frozen organic geochemistry, respectively.

Smear Slide Summary

A table summarizing data from smear slides and thin sections appears on each core-barrel description form. The table includes information on the sample location, whether the sample represents a dominant ("D") or a minor ("M") lithology in the core, and the estimated percentages of sand, silt, and clay, together with all identified components. Note that smear slide analyses tend to underestimate the abundance of foraminifers and volcanoclastic-detrital material because these larger grains are difficult to incorporate into the smear.

Lithologic Description-Text

The lithologic description that appears on each core description form (barrel sheet) consists of two parts: (1) a heading that lists all the major sediment types (see "Sediment Classification" section, this chapter) observed in the core; and (2) a more detailed description of these sediments, including data on color, location in the core, significant features, etc.

Descriptions and locations of thin, interbedded, or minor lithologies are included in the text.

Paleontological Data

Microfossil abundance, preservation, and zone assignment appear on the core description form under the heading "Biostrat. Zone/Fossil Character." The chronostratigraphic unit, as recognized on the basis of paleontological results, is shown in the "Time-Rock Unit" column. Detailed information on the zonations and terms used to report abundance and preservation is presented in the "Biostratigraphy" section (this chapter).

Paleomagnetic, Physical Property, and Chemical Data

Columns are provided on the core description form to record paleomagnetic results (normal, reversed, or unknown polarity, shown as "N," "R," or "?," respectively), physical properties values (wet-bulk density and porosity), and chemical data (percentages of CaCO₃ determined with the coulometrics analyzer). Additional information on shipboard procedures for collecting these types of data appears in the "Paleomagnetism," "Physical Properties," and "Organic Geochemistry" sections (this chapter).

SEDIMENT CLASSIFICATION

The standard DSDP/ODP sediment classification scheme (Supko et al., 1978, with some amendments, was used during Leg 129. Because of the abundance of cherts and porcellanites, extended comments are included on the identification of siliceous sedimentary rocks. A summary of the lithologic classification scheme is shown in Figures 6 through 8. The major component of a sediment type is always listed last in the name, and qualifiers are used as long as the components are present with greater than 25% in smear slides.

Biogenic Sediments

Biogenic sediments are distinguished by biogenic carbonate or/and biogenic silica contents in excess of 30%.

1. Pelagic biogenic oozes contain more than 60% of biogenic components such as nannofossils, foraminifers, radiolarians, diatoms, or silicoflagellates, and are then named appropriately (i.e., siliceous ooze, nannofossil ooze, radiolarian chalk).
2. Transitional biogenic sediments contain 30%–60% biogenic components and more than 40% silt or clay. Sediment names for these materials contain appropriate modifiers (i.e., clayey calcareous ooze or silty limestone).

Pelagic Clays

Pelagic clays which contain less than 30% biogenic components are mainly composed of "residual" pelagic material that accumulated at very slow rates. The various fine-grained components of pelagic clays formed during erosion or non-deposition of biogenic phases include: detrital clay minerals and quartz deposited through eolian transport, authigenic silicates such as clay minerals and zeolites, abundant iron oxides as small aggregates mixed with clays, micronodules of iron and manganese oxides, volcanogenic components (glass, basaltic minerals, palagonite), fish remains, and cosmic particles.

Classification of Siliceous Deposits

Hard sedimentary rocks found during Leg 129 are mainly chert, porcellanite, and limestone. Chert and porcellanite are field terms based on easily observable physical properties; these names are *not* strictly dependent on mineralogy. Cherts and porcellanites can each be composed of either diagenetic quartz (microcrystalline, cryptocrystalline, or chalcedonic varieties) or opal-CT (opal-cristobalite/tridymite). Chert has a

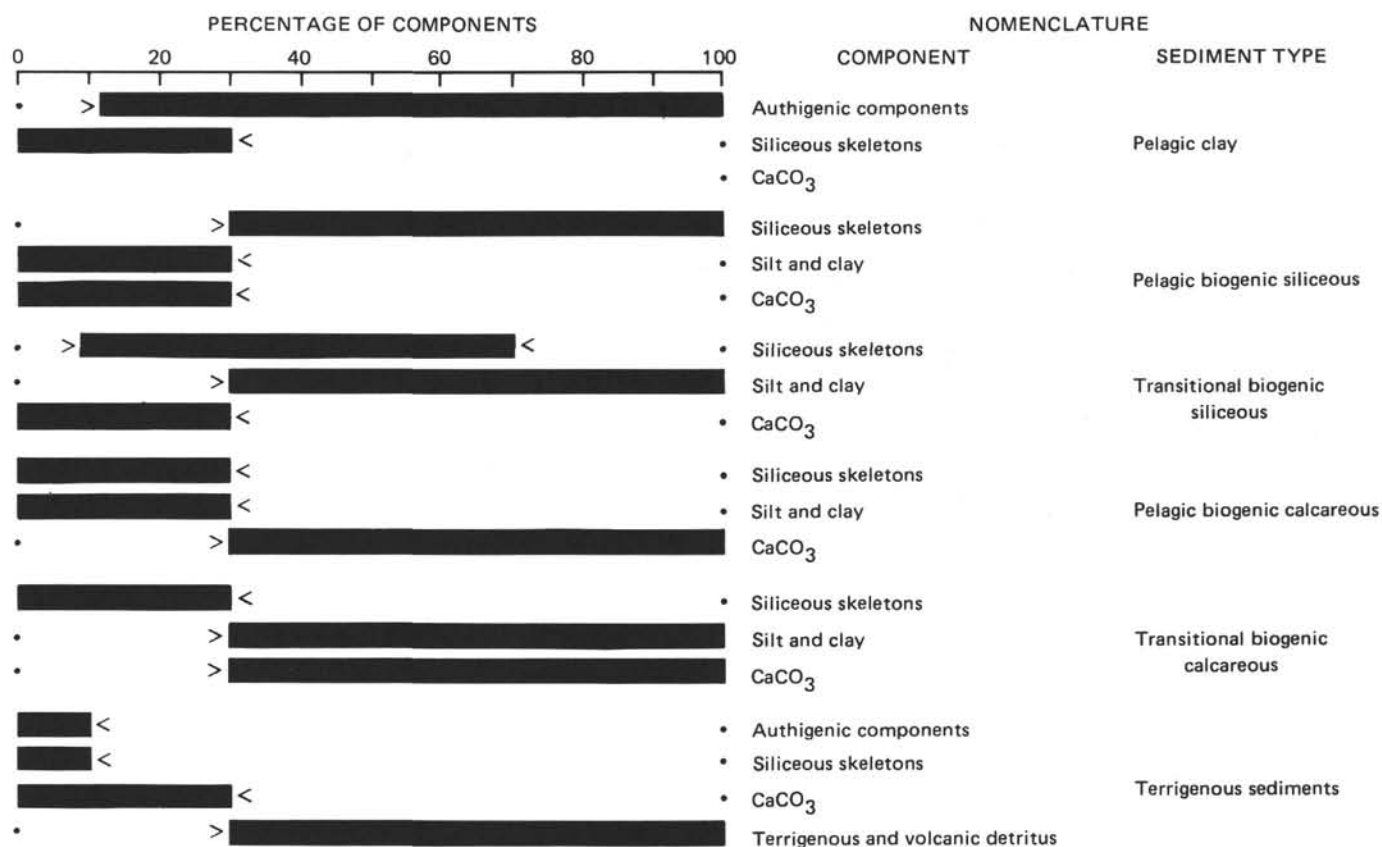


Figure 6. Summary chart of lithologic classification for oceanic sediments used during Leg 129.

glassy to waxy luster, smooth fracture surface, conchoidal fracture, and hardness near 6.3–7.0. Porcellanite has a dull luster, matte to rough surface texture, blocky fracture, and hardness near 4.0–5.5.

Wood- and plastic-handled probes with steel needle tips were used to discriminate between these two lithologies. The steel usually has a hardness of about 5.5–6.0. When a streak of metal was left on a sample scraped with a medium-light stroke, the sediment was named chert. If the sample was gouged by the probe, it was called porcellanite.

Although Leg 129 sedimentologists classified these rocks on their physical properties on the core description form, the principal control on these properties is the ratio of silica/clay (Isaacs, 1982). A ratio of 8:1 or higher is typically needed for a siliceous rock to display cherty characteristics; facies with a ratio less than 8:1 will be a porcellanite or siliceous mudstone (e.g., clayey chert, clayey siliceous ooze, clayey radiolarite). The calcite component has much less effect than clay on the physical characteristics of diagenetic siliceous rocks; a rock with a ratio of 4:1 of silica:calcite may still be chert-like, having a vitreous luster and smooth, conchoidal fracture.

Turbidites

Deposits with graded bedding and locally sharp, scoured bases, cross and planar laminations, and flame structures were described as turbidites. This lithology includes sandstones, siltstones, and claystones (often volcanoclastic) according to the standard grain-size categories and textural classification described earlier (Figs. 6 through 8). A new symbol (T10) was established in the core description form for the normally graded interlayered sand-, silt-, and/or claystones deposited as turbidite beds less than 50 cm thick (Fig. 4).

Volcanogenic Sediments

Volcanogenic rocks were described according to the textural and compositional schemes of Schmid (1981) and Fisher and Schminke (1984). The textural groups are (1) volcanic breccia or agglomerate, greater than 64 mm, (2) volcanic lapillistone or lapilli tuff, 2–64 mm, and (3) volcanic tuff, or ash if un lithified, less than 2 mm in diameter. Tuffs may be composed of various proportions of as vitric (glass), crystal, or lithic particles.

Thickness of Lithologic Units

Thickness of lithologic units defined in the sites reports included unrecovered intervals and were extended downcore until the lithology assigned to the next unit was reached. For example, if only 2 cm of brown clay was recovered in Core 129-800A-1R (0–9.4 mbsf), and the uppermost sediments in the next core contained material assigned to a second unit, then Unit I-Brown Clay would be assigned a thickness of 9.4 m.

BIOSTRATIGRAPHY

The Leg 129 paleontologists chose the following chronostratigraphy for use during the cruise: the time scale of Berggren et al. (1985a, 1985b) for the Cenozoic and the chronostratigraphy and geochronology of Kent and Gradstein (1985), with modifications, for the Early Cretaceous and the Jurassic (Fig. 9).

Preliminary age assignments made on Leg 129 were based mainly on core-catcher samples. Samples from within the cores were examined when fossils were rare or when the need for more a refined age determination seemed necessary. Sample position, abundance, preservation, and age were recorded for each fossil

MILLIMETERS	μm	PHI (Φ)	WENTWORTH SIZE CLASS	
4096		-20		
1024		-12	Boulder (-8 to -12 Φ)	
256		-10		
64		-8	Cobble (-6 to -8 Φ)	GRAVEL
16		-6		
4		-4	Pebble (-2 to -6 Φ)	
3.36		-2		
2.83		-1.75		
2.38		-1.5	Granule	
2.00		-1.25		
1.68		-1.0		
1.41		-0.75		
1.19		-0.5	Very coarse sand	
1.00		-0.25		
0.84		0.0		
0.71		0.25		
0.59		0.5	Coarse sand	
1/2	0.50	0.75		
	0.42	1.0		
	0.35	1.25		
	0.30	1.5	Medium sand	SAND
1/4	0.25	1.75		
	0.210	2.0		
	0.177	2.25		
	0.149	2.5	Fine sand	
	0.125	2.75		
1/8	0.105	3.0		
	0.088	3.25		
	0.074	3.5	Very fine sand	
	0.0625	3.75		
1/16	0.053	4.0		
	0.044	4.25		
	0.037	4.5	Coarse silt	
	0.031	4.75		
1/32	0.020	5.0		
	0.0156	5.25		
	0.0128	5.5	Medium silt	
	0.0078	5.75	Fine silt	
	0.0039	6.0	Very fine silt	MUD
	0.0020	6.25		
	0.00098	6.5		
	0.00049	6.75		
	0.00024	7.0		
	0.00012	7.25		
	0.00006	7.5		
	0.00003	7.75	Clay	

Figure 7. Grain-size categories used for classification of volcanogenic and pelagic sediments (from Wentworth, 1922).

group on core description sheets during examination of each sample, and subsequently combined onto barrel sheets.

Calcareous Nannofossils

Zonation

Cenozoic Zonation

Cenozoic calcareous nannofossil zonation applied during Leg 129 included the schemes of Martini (1971) and Okada and Bukry (1980), both regarded as standard. Calibration of nannofossil zonation with geochronology follows Berggren et al. (1985a, 1985b).

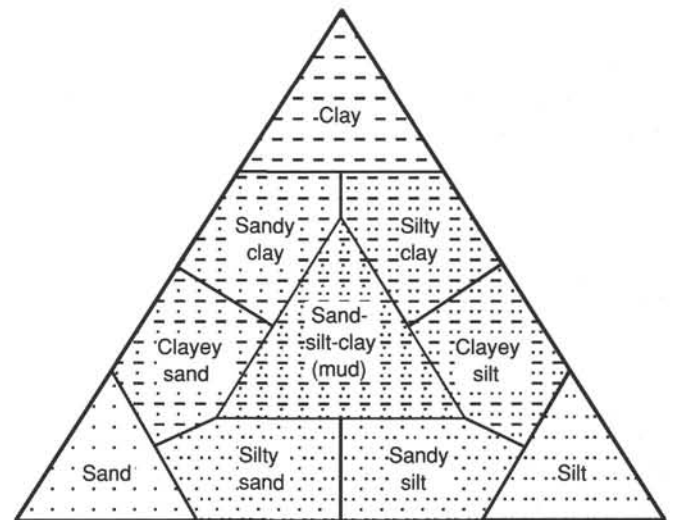


Figure 8. Triangular diagram showing classification scheme used for sedimentary rocks on Leg 129 (after Shepard, 1954).

Mesozoic Zonation

The zonations of Sissingh (1977), Roth (1978), and Thierstein (1976) used in conjunction with the Kent and Gradstein (1985) time scale were applied to Cretaceous sediments (Fig. 9).

For the Early Cretaceous-Late Jurassic interval, modifications proposed by Bralower (1987) and Bralower et al. (1989), who directly calibrated nannofossil events with magnetic anomalies, were adopted.

Methods

Abundance

Total assemblage abundance and species abundances for each sample were estimated by smear slide examination using a light-polarizing microscope at 1250 \times magnification. A letter code was assigned to represent these abundances and presented in the core description forms ("barrel sheets") as follows:

For total abundance, V = very abundant (>50% of the fine fraction), A = abundant (30% to 50% of the fine fraction), C = common (12% to 30% of the fine fraction), F = few (2% to 12% of the fine fraction), R = rare (<2% of the fine fraction), and B = barren.

For species estimates, V = very abundant (more than 10 specimens per field of view), A = abundant (1-10 specimens per field of view), C = common (1 specimen per 2 to 10 fields of view), F = few (1 specimen per 11 to 100 fields of view), and R = rare (1 specimen per 101 to 1000 fields of view).

Preservation

Preservation was estimated by the degree of etching and/or overgrowth of calcareous nannofossils. A letter code was assigned as follows: E = excellent (no evidence of overgrowth or etching), G = good (slight overgrowth and/or etching; nannofossils retained the diagnostic characteristics and could therefore be taxonomically differentiated), M = moderate (overgrowth and/or etching partially altered the ultrastructure of nannofossils but diagnostic features were preserved), and P = poor (overgrowth, etching and/or fragmentation highly altered most nannofossils; only a few could be identified).

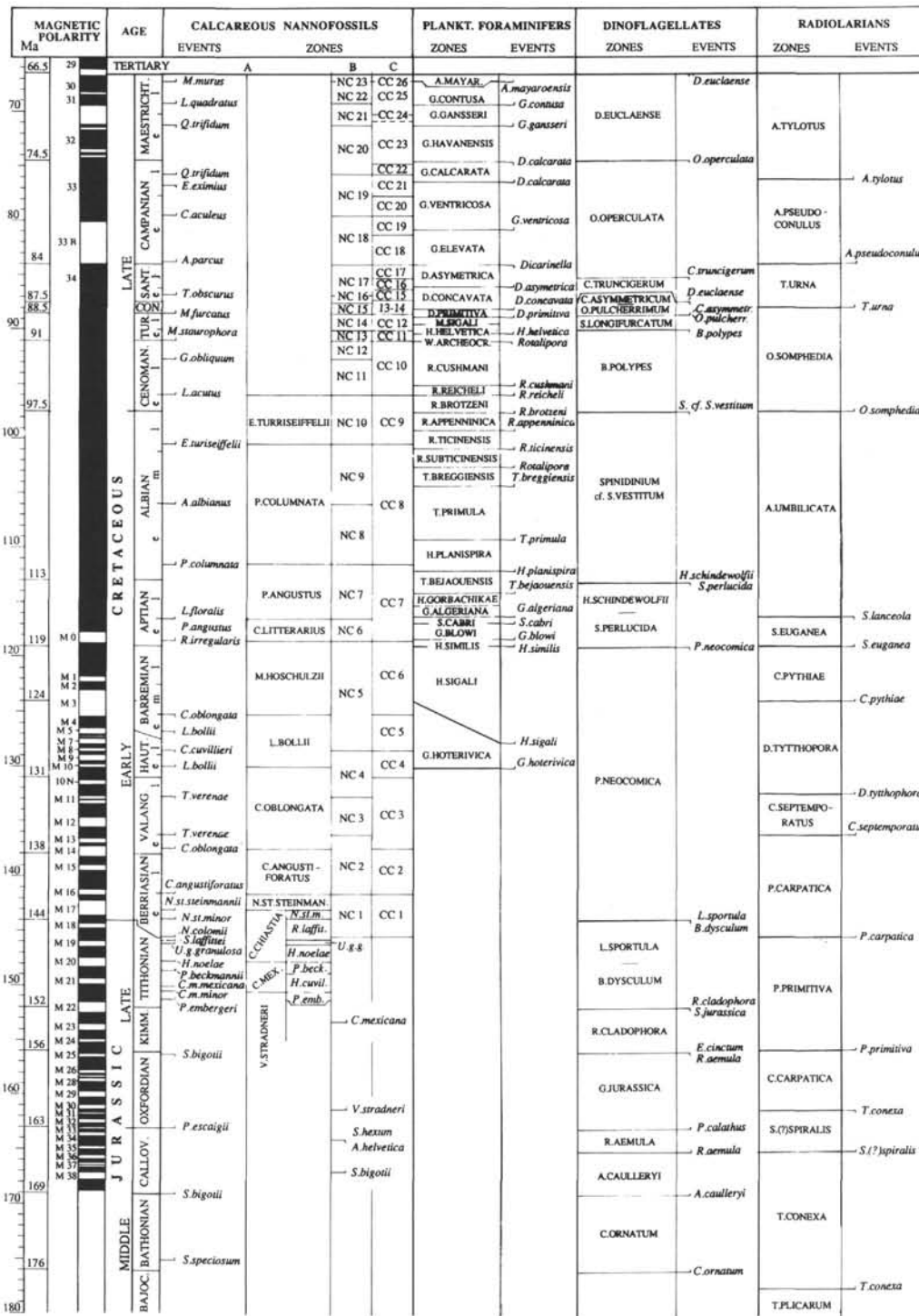


Figure 9. Mesozoic biostratigraphic scheme used during Leg 129. Absolute ages and chronology after Kent and Gradstein (1985). Magnetic sequence after Kent and Gradstein (1985) (Oxfordian p.p.–Maestrichtian; M29–29) and Steiner and Ogg (1988) (Cretaceous–Oxfordian p.p.; M38–M30). The position of the Barremian/Hauterivian boundary is modified after Ogg (1987). The Berriasian/Tithonian boundary is reported following both Kent and Gradstein (1985) (on the left) and new calibration of ammonite zonation (Remane, pers. comm., 1990) (on the right). Subdivisions of stages are based on bioevents; no absolute ages are available for stage subdivisions. Calcareous nannofossil zonation is as follows: (A) Thierstein (1971, 1973, 1976) (Cretaceous and Jurassic), Monechi and Thierstein (1985) (Campanian–Maestrichtian), Bralower (1987) (Valangian–Aptian), and Bralower et al. (1989) (Tithonian–Berriasian); (B) Roth (1978, 1983) (Cretaceous, Jurassic); and (C) Sissingh (1977) (Cretaceous). Planktonic foraminiferal zonation is after Monechi and Thierstein (1985) (late Campanian–Maestrichtian), Kent and Gradstein (1985) (late Aptian–late Campanian), and Caron (1985) (early Hauterivian–late Aptian). Radiolarian zonation is after Sanfilippo and Riedel (1985) (Valangian–Maestrichtian), modifications of Matsuoka and Yao (1985, 1986) (Bajocian–early Valangian). Dinoflagellate zonation is after Williams (1977).

Sample Preparation

Smear slides were prepared for all samples, and investigated with a light-polarizing microscope using transmitted light, phase contrast, and cross-polarized light. Sample preparation was kept simple in order to retain the original nannofossil assemblages. No centrifuge or ultrasonics were applied. A small quantity of sediment was smeared onto a cover glass with a drop of water using a flat toothpick. The suspension was immediately dried on a hotplate. The cover glass was then permanently mounted on a glass slide using optical adhesive and exposed to ultraviolet light for a minimum of 15 min to cure the mounting medium.

Planktonic Foraminifers

Zonation

The zonations of Blow (1969) and Bolli and Saunders (1985) were used for the Neogene. Berggren and Miller's (1988), Bolli and Saunderson's (1985), and Toumarkine and Luterbacher's (1985) zonations were used for the Paleogene. For the Cretaceous the zonations reported by Caron (1985), Kent and Gradstein (1985), and Monechi and Thierstein (1985) were followed. Calibration of planktonic foraminiferal zonation with chronostratigraphy and geochronology followed Berggren et al. (1985a, 1985b) for the Cenozoic and Kent and Gradstein (1985) for the Cretaceous (Fig. 9).

Methods

Abundance

Foraminiferal abundance for each sample as reported in the core description forms ("barrel sheets") was based on the following percentage scales: A = abundant (>20% of the picked sample), C = common (10%–20% of the picked sample), F = few (2%–10% of the picked sample), R = rare (<2% of picked sample), and B = barren.

Preservation

The following terms were used to describe the state of foraminiferal preservation: E = excellent (specimens complete with well preserved fine detail), G = good (some specimens fractured or distorted but with good preservation of fine detail), M = moderate (specimens fractured or distorted, and lacking some fine detail), and P = poor (specimens fractured or distorted, fine detail absent or overgrown).

Sample Preparation

Samples of approximately 20 cm³ were processed for foraminifers by kiln-drying the samples and treating with a 1% Calgon solution. Samples were then wet-sieved through a 38- μ m screen and oven-dried. Residues were divided as necessary with a microsplitter and hand-picked for all foraminifers greater than 38 μ m in size. Specimens were mounted in 64 cell reference slides.

Radiolarians

Zonation

Cenozoic Zonation

Radiolarian zonal assignments of Cenozoic samples were based on the tropical zonation of Riedel and Sanfilippo (1978) and subsequent modification in Sanfilippo et al. (1985). Calibration of this zonation with chronostratigraphy and geochronology follows Berggren et al. (1985a, 1985b).

Mesozoic Zonation

Figures 9 and 10 show the radiolarian zonation scheme adopted during Leg 129 for Middle Jurassic to Cretaceous sediments and the calibration with the geochronology of Kent and Gradstein (1985). The zonation of Sanfilippo and Riedel (1985) was applied to the Cretaceous sediments except for the Berriasian and early Valanginian. For the Middle Jurassic to early Valanginian interval, the radiolarian zonation of Matsuoka and Yao (1985, 1986) was adopted with modifications. The lowermost Cretaceous *Pseudodictyomitra carpat-ica* Zone is here defined as an interval zone, although it was originally defined as an assemblage zone (Matsuoka and Yao, 1985). Its base and top are limited by the first occurrences of *P. carpat-ica* and *Cecrops septemporatus*, respectively. The top of the uppermost Jurassic *Pseudodictyomitra primitiva* Zone is defined by the first occurrence of *P. carpat-ica*.

Age determinations of sediments for the Middle Jurassic to early Valanginian interval are tentative because radiolarian zones of this interval are not sufficiently dated by other age diagnostic fossils. Age assignments of sediments depended largely on correlation of Matsuoka and Yao's zonation with Baumgartner's (1984, 1987) zonation. His zonation was based primarily on his research of Atlantic and Mediterranean Tethys regions where radiolarian-bearing sequences contain other age diagnostic fossils.

Methods

Abundance

Total abundance of radiolarians was estimated on strewn slides of sieved acid residues. Abundance was recorded on the core description forms ("barrel sheets") as follows: A = abundant (>1000 radiolarians per slide), C = common (101–1000 radiolarians per slide), F = few (11–100 radiolarians per slide), R = rare (1–10 radiolarians per slide), and B = barren.

Preservation

Preservation of radiolarian tests in strewn slides was defined as follows: G = good (no or little signs of dissolution and/or fragmentation), M = moderate (dissolution and/or fragmentation evidently observed, but not heavy), and P = poor (dissolution and/or fragmentation effect).

Sample Preparation

Strewn slides were prepared and examined for each core catcher and occasionally from other stratigraphic intervals as well. Unconsolidated sediment samples were boiled in Calgon for 5–20 min. Consolidated samples were disaggregated using 5% hydrofluoric acid (HF) for 12–24 hr. The time of treatment varied depending on the degree of induration of the sediments. Carbonate-rich samples were first decalcified in 10% hydrochloric acid (HCl). The samples were sieved and the >46- μ m fraction was examined. The residues, including radiolarian tests, were mounted in Norland Optical Adhesive or Entellan New according to the refractive index of the tests.

Palynomorphs

Zonation

At present no standard dinoflagellate zonation is available for the Mesozoic and Cenozoic of the Pacific. Ages are mainly based on the dinoflagellate zonation scheme of Williams (1977). The zones of Williams (1977) are based on range zones, concurrent zones, and well-defined acme zones (Hedberg, 1976). The adopted zonation is correlated to the geochronol-

Age		Sanfilippo and Riedel (1985)	Baumgartner (1984, 1987)	Matsuoka and Yao (1985, 1986)	This report		
Cretaceous	Late	Maestrichtian	<i>A. tylotus</i>		<i>A. tylotus</i>	<i>A. tylotus</i>	
		Campanian	<i>A. pseudoconulus</i>		<i>A. pseudoconulus</i>		<i>A. pseudoconulus</i>
		Santonian Coniacian	<i>T. urna</i>		<i>T. urna</i>		
		Turonian					
		Cenomanian	<i>O. somphedia</i>		<i>O. somphedia</i>		<i>O. somphedia</i>
	Early	Albian	<i>A. umbilicata</i>		<i>A. umbilicata</i>		
		Aptian	<i>S. euganea</i>		<i>S. euganea</i>	<i>S. lanceola</i> <i>S. euganea</i>	
		Barremian	<i>C. pythiae</i>		<i>C. pythiae</i>	<i>C. pythiae</i>	
		Hauterivian	<i>D. tythopora</i>		<i>D. tythopora</i>	<i>D. tythopora</i>	
		Valanginian	<i>C. septemporatus</i>	E2		<i>C. septemporatus</i>	<i>C. septemporatus</i>
				E1			
		Berriasian		D	<i>P. cf. carpatica</i>	<i>P. carpatica</i>	<i>P. carpatica</i>
Jurassic	Late	Tithonian		C2			
		Kimmeridgian		C1	<i>P. primitiva</i>	<i>P. primitiva</i>	<i>P. primitiva</i>
		Oxfordian		B	<i>C. carpatica</i>	<i>C. carpatica</i>	<i>T. conexa</i> <i>S.(?) spiralis</i>
	Middle	Callovian		A2	<i>S.(?) spiralis</i>	<i>S.(?) spiralis</i>	
		Bathonian		A1	<i>T. conexa</i>	<i>T. conexa</i>	
				A0			<i>T. conexa</i>
		Bajocian			<i>T. plicarum</i>	<i>T. plicarum</i>	

Figure 10. Mesozoic radiolarian zonation and age assignment used during Leg 129. The zonation of Matsuoka and Yao (1985, 1986) was not originally assigned to stages.

ogy of Berggren et al. (1985a, 1985b) for the Cenozoic and to the time scale of Kent and Gradstein (1985) for the Mesozoic (Fig. 9).

Methods

Abundance

The abundance of palynomorphs per slide was registered in the core description forms ("barrel sheets") as follows: A = abundant (>1000), C = common (100–1000), F = few (10–100), and R = rare (1–10).

Preservation

Palynomorph preservation was reported as follows: G = good (>75% undamaged specimens, i.e., oxidized, broken, or folded), M = moderate (25%–75% undamaged specimens), and P = poor (<25% undamaged specimens).

Sample Preparation

The samples were treated with 35% HCl and sieved through a 17- μ m sieve to remove fine sand and clay. After sieving the residue was put in a watch glass. Rotation of the

watch glass concentrated the palynomorphs in the upper and middle part of the solution, where they could be extracted with a pipette. In addition, cherts were treated with 40% HF to dissolve the silicates and then sieved through a 10- μ m mesh. Samples were mounted with glycerine jelly.

PALEOMAGNETISM

Measurements of natural remanent magnetization (NRM) and volume magnetic susceptibility (K_v) were performed aboard ship. Progressive demagnetization was undertaken to obtain the characteristic remanent magnetization (ChRM) of the rocks. Aboard ship, alternating field (AF) demagnetization was the only practical method for examining ChRM because of the time factor; the automated AF demagnetization and measurement equipment embodied in the pass-through magnetometer system aboard ship allows a rapid examination of all core material as it is recovered. Most recovered core was measured in this manner, but consequently, no time was left for discrete sampling and demagnetization.

Instruments

A 2G Enterprises (Model 760R) 3-axis, pass-through cryogenic rock magnetometer was available for measurement of remanence aboard the *JOIDES Resolution* during Leg 129. AF demagnetization equipment (Model 2G600) capable of alternating fields up to 25 mT is integrated with the cryogenic magnetometer. Communications between cryogenic sensors, the AF degaussing system, and the drive motor moving the core were linked through a FASTCOM4 multiserail communications board in an IBM PC AT-compatible computer; all devices and actual measurements of core were controlled by a modified version of the Rhode Island University BASIC program. Leg 129 modifications to this program included superconducting quantum interference devices (SQUID) control commands such that the magnetometer could operate at the $1\times$ scale with flux counting for sediments and $100\times$ for basalts. The spinner magnetometer was not used during Leg 129.

The sensors in the cryogenic magnetometer measure magnetization over an interval of approximately 20 cm. Each axis has a slightly different response curve. The widths of the sensor regions are such that up to 150 cm³ of core contributes to the sensor response at any measurement instant. The large volume of core material within the sense region permits determination of remanence for even weakly magnetized samples despite the relatively high background noise related to the motion of the ship.

Sediments

Remanence measurements of sediments were performed by passing archive-half sections through the cryogenic magnetometer. In cores where recovery consisted of discrete fragments, these fragments were taped in the magnetometer tray with bedding planes perpendicular to the magnetometer's "z" axis; to compensate for the size of the sense region, samples were separated by 10 cm. Depending on the lithology, measurements were taken at 2-, 3-, or 5-cm spacings. The AF strengths used also depended on lithology; generally, most core segments were demagnetized to 15 mT.

Basalts

Basalts from Leg 129 were measured in much the same fashion as the sediments. Basalt cores generally were run as whole sections. The excessive weight of the whole sections occasionally required that they be divided into two (or three) parts and run separately; this required individual pieces to be taped into the magnetometer tray, spaced apart as described for the chert fragment measurements. More detailed AF

demagnetization steps were used for the basalts than for the sedimentary rocks, again generally concluding with 15 mT.

Magnetic Susceptibility Measurements

Magnetic susceptibility was measured for Sites 801 and 802. A Bartington Instruments magnetic susceptibility meter (model M.S.1) with an M.S.1/CX 80-mm whole-core sensor loop set at 0.47 kHz (range 1) was used for sediment measurements. The susceptibility meter is on-line with the GRAPE and *P*-wave logger on the MST. Igneous rock susceptibility was measured using the type MS1B sensor unit. Whole cores were measured, prior to splitting. Only those cores having sufficient volume recovery were run.

INORGANIC GEOCHEMISTRY

Interstitial Water Sampling and Chemistry

Shipboard interstitial water analyses were performed on 5- to 10-cm-long whole-round sections that were cut from the core immediately after it arrived on deck. Interstitial waters were obtained by squeezing using a titanium and stainless steel piston modified after Manheim and Sayles (1974). Before squeezing, the core surfaces were carefully scraped with a spatula to remove the potentially contaminated exterior of the sample. Then the core was placed into the piston and squeezed using a hydraulic press at pressure up to 240 MPa. The water was collected in a plastic syringe and filtered through a 0.2- μ m disposable filter.

Interstitial water samples were routinely analyzed for alkalinity, pH, and salinity and for chlorine (Cl), sulfate (SO₄), calcium (Ca), and silicon (Si) concentrations using the analytical technique described in Gieskes and Peretsman (1986). Magnesium (Mg), potassium (K), manganese (Mn), and strontium (Sr) concentrations were measured via atomic absorption. Most measurements were calibrated on the International Association of Physical Sciences Organizations (IAPSO) standard seawater. Results are expressed in milli- or micromole per liter of solution, taking 1.024 g/cm³ for the density of sample water. Sodium concentrations were calculated by charge balance (Na⁺); the difference between calculated salinity using Na⁺ data and measured salinity never exceeds 3%. Chemical data are reported in tables in each site chapter in this volume. Sub-bottom depths given have been rounded to the nearest meter.

Alkalinity and pH were determined using a Metrohm autotitrator with a Brinkmann combination pH electrode. Alkalinity reproducibility is better than 5%; data are given in millimoles of acid equivalent per liter.

Salinity was determined using a Goldberg optical hand refractometer measuring the total dissolved solids. Values are given in weight per mil.

Chlorinity was measured by silver nitrate titration of 0.1 mL of sample diluted in 5 mL of deionized water using potassium chromate as an indicator. Reproducibility on the IAPSO standard is better than $\pm 0.6\%$.

Sulfate concentration was measured by ion chromatography. Samples of 0.1 mL diluted to 50 mL with deionized water were used. Reproducibility on different dilutions of the IAPSO standard is better than $\pm 2\%$.

Calcium was determined by titration of a 0.5-mL sample with EGTA using GHA as an indicator. Near the endpoint, the Ca-GHA complex was extracted into a layer of butanol to enhance the precision. No correction was made for Sr that is included in the results. Reproducibility is $\pm 0.7\%$ on the IAPSO standard.

Silica was determined by production of silicomolybdate complex and its reduction to give a blue color on a 0.1-mL

sample. Absorption was measured at 812 nanometers. Reproducibility is $\pm 3\%$.

Atomic absorption measurements were done with a Varian SpectrAA-20 spectrophotometer to determine Mg, Mn, K, and Sr concentrations. All measurements were done in absorption mode using an oxidizing air-acetylene flame.

Magnesium was analyzed on 1:1,000 to 1:10,000 solutions of the samples. Lanthanum trichloride (10,000 ppm) was used as a realizing agent in the sample solution and in the standards. Reproducibility varies from $\pm 0.5\%$ at 54 mmol/L concentration to $\pm 2\%$ at 5 mmol/L concentration.

Potassium was determined on 1:100 to 1:500 sample solutions with 1,000 ppm cesium chloride as ionization suppressor. Reproducibility is $\pm 3\%$.

Strontium concentrations were measured on 1:10 to 1:50 solutions of the samples. Lanthanum trichloride (10,000 ppm) was used as a realizing agent in the sample solution and in the standards. Reproducibility is better than $\pm 2\%$.

Manganese concentrations were analyzed on 1:5 solutions of the samples without releasing agent. Reproducibility is better than $\pm 2\%$.

Carbonate, Organic Carbon, and Sulfur Content Determinations

Samples of both sediment and basaltic crust were analyzed aboard ship for inorganic carbon, total carbon, and sulfur. Analyses are presented in the "Sedimentology" and "Igneous Petrology" sections of the site chapters in this volume. Sediment CaCO_3 data are reported on the core description forms ("barrel sheets"). Measurements were done on most of the samples used for physical properties measurements, on samples of the interstitial water squeeze-cake, and on some additional samples. All samples were about 10 cm³ in size and were freeze-dried prior to powdering. Samples were weighed with a Cahn 29 Automatic Electrobalance, which averages a total of 50 weight measurements to compensate for ship heave. Organic carbon is calculated as the difference between total carbon and inorganic carbon. Results are expressed in weight percent (wt%). Inorganic carbon is expressed in wt% equivalent of CaCO_3 .

Total inorganic carbon concentrations were obtained using a coulometric 5011 Coulometer equipped with a system 140 carbonate carbon analyzer. About 60 mg of each sample was reacted in 2-ml 2N HCl solution; the liberated CO_2 was carried into a coulometric cell where it reacted in a monoethanolamine solution with a colorimetric indicator. The change in absorbance was monitored by a photocell. Frequent blank and standard runs indicated a relative error of $\pm 1\%$.

Total carbon and sulfur content were determined using a CNS Carlo Erba analyzer NA 1500. Vanadium pentoxide was added to a sample of about 30 mg in a tin container, which was flash-combusted at more than 2000°C in an oxygen atmosphere. The oxidized species were driven by a helium flux through (1) an oxidation catalyst, (2) a copper reduction reactor to remove O_2 and transform SO_x into SO_2 , (3) a Mg perchlorate filter to remove H_2O , (4) a chromatographic column to separate the different gases, and (5) a thermal conductivity detector to measure the concentrations of gases. Blanks, standards, and duplicates give a reproducibility of $\pm 1\%$ and $\pm 0.02\%$ as a limit detection level.

PHYSICAL PROPERTIES

Shipboard measurement of physical properties provides information that aids characterization of lithologic units, allows verification of downhole geophysical logging results, and provides constraints on interpretation of seismic reflection and other geophysical data. Furthermore, these data are used

in paleoceanographic interpretation of sedimentary units, heat-flow calculations, and determination of the mechanical state of sediments and rocks.

Physical properties measurements made on cores recovered during Leg 129 included index properties, compressional-wave velocity, and thermal conductivity. Samples were chosen to be representative of the core or section as a whole, and were taken in areas of least disturbance. Sample selection and spacing depended on the core recovery and the thickness and homogeneity of the recovered sequences. All measurements were conducted on discrete samples taken from split cores, with the exception of thermal conductivity measurements of soft sediments that were made at discrete intervals in whole-round core sections. Continuous measurements of wet-bulk density and compressional-wave velocity, provided by the gamma-ray attenuation porosity evaluator (GRAPE) and IOS compressional-wave core logger (*P*-wave logger) incorporated in the multisensor track, were not made because sediments and rocks typically did not completely fill core liners, or, in the recovery of soft sediments, because the cores were too highly disturbed by rotary coring.

Compressional-Wave Velocity

Compressional-wave velocity measurements were taken on discrete samples that were sufficiently competent to provide adequate signal strength. All velocity measurements were made at atmospheric pressure and involved the determination of the traveltime of a 500-kHz compressional wave through a measured thickness of sample, using a Hamilton Frame Velocimeter and Tektronix DC 5010 counter/timer system. Samples of soft sediment were taken with a parallel-sided sampling tool or carefully cut from the cores. A double-bladed diamond saw was used to cut samples from lithified sediments and basement rocks. Sample thickness was measured directly from the velocimeter-frame lead screw. Zero traveltimes for the velocity transducers were estimated by linear regression of traveltime vs. distance for a series of aluminum and lucite standards. Filtered seawater was used to improve the acoustic contact between the sample and the transducers. Estimated accuracy of the velocity measurements is $\pm 2\%$ (Boyce, 1976). Compressional-wave velocity was measured for both vertical (perpendicular to bedding) and horizontal (parallel to bedding) propagation directions for all samples that were large enough and sufficiently indurated to be cut perpendicular to bedding with the double-bladed saw. Velocity anisotropy was calculated from the vertical velocity (V_v) and horizontal velocity (V_h) values following the expression of Carlson and Christensen (1979), where anisotropy (A) is given as the ratio of velocity difference to mean velocity, expressed as a percentage:

$$A = 200(V_h - V_v)/(V_h + V_v). \quad (1)$$

Igneous rocks were treated differently than sedimentary rocks. The curatorial procedures required for igneous rocks involved drying the samples, which may increase measured velocities by as much as 8% (Hay et al., 1984). Samples cut from the cores were placed in sea water for several hours prior to velocity and index properties measurements in an attempt to resaturate the rock and minimize the drying-induced error.

Index Properties

Index properties (bulk density, grain density, water content, and porosity) were calculated from measurements of wet and dry weights and dry volume. Wet-bulk density was also determined using the GRAPE special 2-min count technique (Boyce, 1976). Samples of approximately 10 cm³ were taken

for gravimetric determination of index properties. Soft sediment samples were placed in precalibrated aluminum containers prior to weight and volume measurements. Index properties measurements for lithified sediment and basement rock samples were made using sample cubes cut for velocity determinations. The calibrated aluminum containers were not used for weight and volume measurements for the cubes because these samples were larger than the containers. Sample weights were determined aboard ship to a precision of ± 0.01 g using a Scitech electronic balance. These measurements were repeatable within ± 0.04 g. Wet and dry volumes were determined using a Quantachrome helium-displacement Penta-Pycnometer. Volumes of soft sediment samples were determined using the pycnometer's small sample chamber inserts, whereas volumes for the cube samples were determined in the large-capacity chambers. At Sites 800 and 801, a 70-cm³ displacement volume was added to the chambers to reduce the empty volume and associated measurement error. Volumes of cube samples from Site 802 were measured using inserts fabricated to more closely match the dimensions of the cubes and displace a greater volume in the large-capacity chambers. The Quantachrome pycnometer measures volumes to an approximate precision of 10^{-4} cm³. Measurements were typically repeatable to ± 0.05 cm³ using the small chamber inserts and ± 0.05 – 0.10 cm³ using the large-capacity chambers. Use of the inserts designed for cube samples improved the accuracy of volume determinations for the cubes. Dry weight and volume measurements were obtained after the samples were oven-dried at 105°C for 24 hr and allowed to cool in a desiccator. All weight and volume measurements were performed in triplicate and averaged to obtain the values

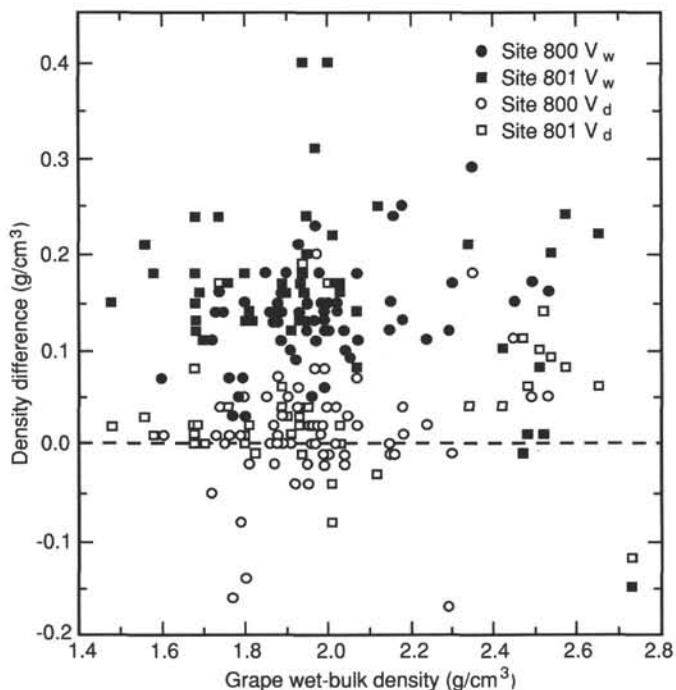


Figure 11. Density difference (gravimetric wet-bulk density – GRAPE wet-bulk density) vs. GRAPE wet-bulk density. Density differences calculated from wet-bulk densities obtained from wet volume measurements are represented by filled circles and squares. Density differences calculated from estimates of wet volume derived from dry volume, dry weight, and wet weight measurements are represented by open circles and squares.

used in calculating index properties. A salt correction assuming 35 ppt interstitial fluid salinity was applied to density and porosity computations as per Hamilton (1971).

Wet-bulk density was also determined using the GRAPE special 2-min count technique as described by Boyce (1976). The GRAPE measurements were made perpendicular to bedding on half-round samples cut from the cores using the double-bladed saw. All counts for the samples and accompanying air (background) counts were made in duplicate and averaged. Grain density values from gravimetric measurements were used to correct the wet-bulk density determined by the GRAPE for deviation of the grain density of the sample from that of quartz. The precision estimated for this technique is $\pm 1.5\%$ (Boyce, 1976). Wet-bulk density values determined by the 2-min GRAPE technique were used to estimate porosity of samples for which gravimetric measurements were not made. Porosity (ϕ) was estimated by assuming a value for grain density (δ_s) and using the relationship:

$$\phi = (\delta_s - \delta_{bw}) / (\delta_s - \delta_f) \quad (2)$$

where δ_{bw} is wet-bulk density determined by the GRAPE and δ_f is interstitial fluid density, which is assumed to equal 1.024 g/cm³.

Determination of wet-bulk density by gravimetric techniques was initially based on measurement of wet weight (W_w) and wet volume (V_w) and calculated using the relationship:

$$\delta_{bw} = W_w / V_w \quad (3)$$

Comparison of the wet-bulk density calculated using equation 3 with that determined by the GRAPE 2-min technique revealed that gravimetric determinations were consistently higher than GRAPE measurements (Fig. 11). The difference between wet-bulk densities determined by the two methods was resolved to be a result of anomalously low wet volume measurements. This source of error was indicated by samples for which the measured wet volume was less than the dry volume and situations in which the calculated wet-bulk density was greater than the grain density. Because of the wet volume measurement errors the calculation of wet-bulk density was changed to include an estimate of wet volume derived from dry volume (V_d), wet weight, and dry weight (W_d) measurements according to the relationship:

$$V_w = V_d + (W_w - W_d) / \delta_f \quad (4)$$

where δ_f is the density of evaporated water and assumed to equal 1. The dry volume, V_d , includes both the volume of the sediment or rock constituents and the volume of salt remaining in the sample upon drying. Wet-bulk densities calculated using the above relationship more nearly approximate those obtained using the GRAPE (Fig. 11).

Dry volume measurement errors were encountered in measurements of low porosity cherts and igneous rocks. These errors were manifested as anomalously high dry volumes and low grain densities. The errors were overcome by crushing samples, determining the grain density of the powdered samples, and using the grain density and water content to estimate the dry volume and by increasing the helium purge time for the pycnometer from 2 min to 4 min.

Thermal Conductivity

The thermal conductivity measurement techniques used during Leg 129 are described by Von Herzen and Maxwell

(1959) and Vacquier (1985). Measurements were made with a Thermcon-85 unit, and all data are reported in units of $W/m \cdot K$. The estimated error in the measurements is about 5%–10%. All data were corrected for *in-situ* pressure and temperature (Ratcliffe, 1960), assuming hydrostatic pressure and a conductive thermal gradient of about $35^{\circ}C/km$.

Soft Sediment "Full-space" Measurements

To reduce background thermal transients, cores were allowed to equilibrate in their liners until the sediments reached a temperature near that in the lab. A needle probe was inserted in every other section, through holes drilled through the liners. New thermal conductivity software, introduced during Leg 129, allowed the user to monitor sample temperatures (using the thermistors in the needle probes) without applying a current to the heater wires. The actual test sequence can then be delayed until after the background temperature drift in all samples has been reduced to some arbitrary level (in this case $0.04^{\circ}C/min$). Once the samples are fully equilibrated, the heater circuit is closed and the temperature rise of the probes is recorded. Thermal conductivity is calculated from the rate of temperature rise in the probe while a heater current is flowing.

After the heater has been on for about 60 s, the needle probe response is very close to that of a line source with a constant heat generation per unit length. We always used the time interval of 60 to 240 s after the heater was turned on. The temperature rise in the probe should vary logarithmically with time as:

$$T(t) = (q/4\pi k) \ln(t) + \text{const.} \quad (5)$$

where k is the thermal conductivity, T and t are the temperature and time, respectively, and q is the heat generated per unit length of the probe. From equation 5, the thermal conductivity is derived from the slope of temperature vs. the logarithm of time. When the sediment became too firm to allow easy insertion of the probe, we tested half-round samples, as described below.

Hard Rock "Half-space" Measurements

Thermal conductivity measurements on lithified sediments and rocks were conducted on split cores using the half-space technique (Vacquier, 1985). With this method a rock sample with one flat surface is placed on top of a needle probe that is embedded along the surface of a slab of low conductivity material. The flat surface of the sample is polished with sandpaper to minimize pockets of water or air and thus to assure good contact with the slab containing the needle probe. EE&G thermal conducting compound was also used to improve the thermal contact between the slab and the sample. The sample and needle are immersed in a water bath to maintain a uniform temperature, to avoid cooling by evaporation, and to keep the sample saturated. The data reduction procedure for the half-space method is exactly the same as for

the full-space method except that the data must be corrected to account for the geometry of the experiment.

The original ODP half-space water bath was constructed (on Leg 106) out of a standard thermal conductivity needle probe, a block of epoxy, and a plastic wash basin. The epoxy block was fixed to the bottom of the basin, and the probe was inserted through a hole cut in the side of the basin so that the needle fit in a groove on the top of the epoxy block. The upper surface of the needle was exposed so that the probe would be sandwiched between the sample and the epoxy block. During the early part of Leg 129 we built a larger bath with three probes and epoxy bases so that several samples could be tested at one time.

Because the geometry of the half-space experiment is not perfect (i.e., the needle is never positioned exactly between the sample and epoxy, the sample is not semi-infinite, there is never an ideal thermal contact, the EE&G thermal compound is a heat sink), each block/needle pair was separately calibrated over fixed time intervals. We chose an interval of 60–240 s because (1) before 60 s the temperature vs. $\log(\text{time})$ data rarely vary linearly, and (2) after about 240 s the thermal front from the heated needle tends to "feel" the edge of the smaller, more conductive samples. We conducted several hundred experiments with 4 standards in full-space and half-space configurations to establish an empirical relationship between the two (Table 1 Fig. 12). The standard with the highest conductivity, macor, has a conductivity of about $1.61 W/m \cdot K$, which is lower than the conductivities of some of the samples. Sample conductivities greater than $1.61 W/m \cdot K$ thus required that we extrapolate past the range of the standards; these measurements probably have the highest errors.

The following full-space conductivities were determined for each standard (\pm standard deviation) in full-space configuration using a time interval of 60–240 s: black rubber = $0.544 \pm 0.015 W/m \cdot K$ ($n = 8$), red rubber = $0.967 \pm 0.048 W/m \cdot K$ ($n = 27$), fused silica = $1.536 \pm 0.055 W/m \cdot K$ ($n = 28$), macor = $1.752 \pm 0.058 W/m \cdot K$ ($n = 27$). The fused silica and macor values are both higher than determined elsewhere (1.38 and $1.61 W/m \cdot K$, Vaquier, 1985; Shipboard Scientific Party, 1989; M. Langseth, pers. comm., 1989; A. Fisher, unpubl. data), possibly because we were forced to use a lot of the EE&G thermally conductive compound to assure a good contact between the needle and the standards. The excess compound probably acted as a heat sink, simulating unrealistically high conductivities in the full-space tests with fused silica and macor. We did not have this problem with the rubber standards because these materials tend to grip the needles.

We converted half-space values to full-space conductivities by using a least-squares best-fit of the data to derive a linear equation of the form: full-space conductivity = $A + B$ (half-space conductivity). Previously determined full-space conductivities for fused silica and macor were used in these regressions.

IGNEOUS ROCKS

Core Curation and Shipboard Sampling

Igneous rocks are split into archive and working halves using a rock saw with a diamond blade. The petrologists decide on the orientation of each cut so as to preserve unique features and/or expose important structures. The archive half is described, and samples for shipboard and shore-based analyses are removed from the working half. Each piece is numbered sequentially from the top of each section, beginning with the number 1. Pieces that can be fitted together (like a

Table 1. Half-space thermal conductivity standards.

Probe	Black rubber	Red rubber	Fused rubber	Macor
1	0.340 ± 0.004	0.508 ± 0.013	0.693 ± 0.018	0.825 ± 0.026
4	0.305 ± 0.004	0.478 ± 0.009	0.661 ± 0.017	0.794 ± 0.024
9	0.333 ± 0.005	0.520 ± 0.009	0.725 ± 0.015	0.864 ± 0.008
211	0.315 ± 0.004	0.496 ± 0.024	0.679 ± 0.018	0.838 ± 0.029

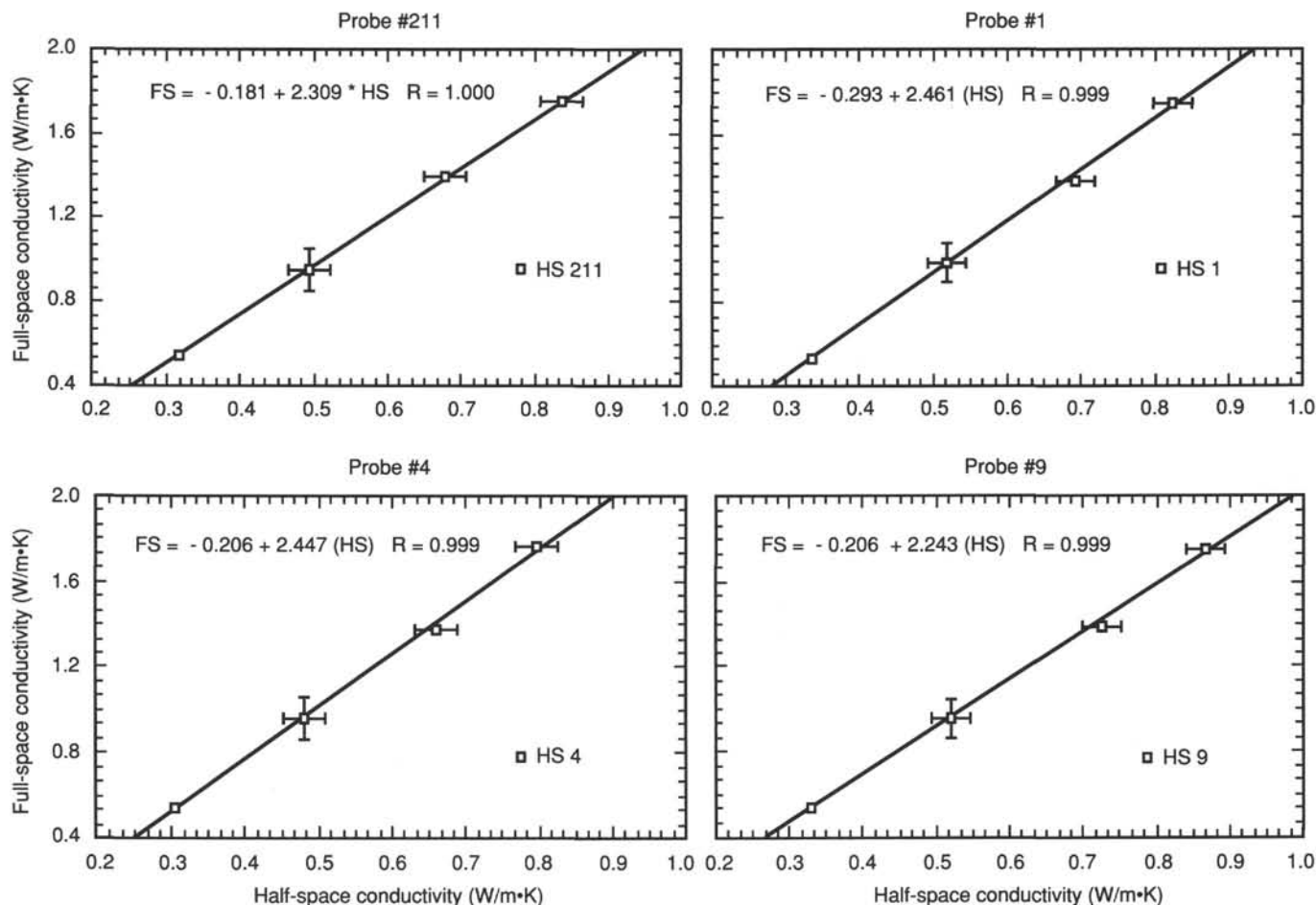


Figure 12. Full-space vs. half-space conductivities of four standards measured with four needle-probe/epoxy-block pairs. The four standards are, in order of increasing conductivity, black rubber, red rubber, fused silica, and macor. The conductivities of fused silica and macor are widely known; the exact composition of the black and red rubber is not known, and their conductivities were determined during Leg 129. In all cases, conductivities were determined over a time interval of 60–240 s. In each plot, the error bars indicate 1 standard deviation of all measurements made during Leg 129. The least squares best fit is also shown.

jigsaw puzzle) are assigned the same number, but are lettered consecutively (e.g., 1A, 1B, 1C, etc.). Spacers are placed between pieces with different numbers, but not between those with different letters and the same number. The presence of a spacer may represent a substantial interval of no recovery. Whenever the original unsplit piece is sufficiently large that the top and bottom can be distinguished before removal from the core liner (i.e., the piece could not have rotated about a horizontal axis in the liner during drilling), a red wax cross is marked on the base of each piece.

Before the rock is dry, sampling is carried out for shipboard physical properties, magnetics, XRD, and thin-section studies. Minicores are taken from the working half and stored in seawater prior to physical properties measurements. Non-destructive measurements of magnetic susceptibility and sometimes thermal conductivity are made on the archive half of the core. The archive half is next described in detail on the VCD form and finally photographed before storage.

Visual Core Descriptions

Hard rocks sampled from the basement are graphically represented on VCD forms specific to igneous and metamor-

phic rocks (see “Site Summary” appendices, this volume). Copies of the VCD forms, as well as other prime data collected during Leg 129 are available on microfilm at all three ODP repositories. The left-hand column of the VCD (Fig. 13) is a graphical representation of the archive half. A horizontal line across the entire width of this column denotes a plastic spacer glued between rock pieces inside the liner. The number of each piece is also recorded, with oriented pieces indicated by the presence of an upward-pointing arrow to the right of the relevant piece. Shipboard samples and studies are indicated in the “shipboard studies” column, using the following notation: XRD = X-ray diffraction analysis, PM = magnetic measurements, TSB = thin-section billet, and PP = physical properties measurement.

When cores are described, checklists of macroscopic features are used to ensure consistent and complete descriptions, one for fine- and medium-grained extrusives and dikes, and another for plutonic rocks. The VCD form for fine- and medium-grained igneous rocks requires the following information:

1. The leg, site, hole, core number and type, and section number.

129-801C-1R-3

UNIT 1: APHYRIC MICRODOLERITE GRADING TO SPARSELY PLAGIOCLASE PHYRIC BASALT

Pieces 1A-1G

CONTACTS: Not actually observed, but grain-size fines towards the bottom (cut by veinlet).
PHENOCRYSTS:
 Plagioclase - 1%; c.1.0; euhedral/subhedral laths, altered to white and green clays.
GROUNDMASS: Holocrystalline to hypocrySTALLINE, particularly at bottom. Medium to fine grained, fining towards the bottom.
VESICLES: None observed.
COLOR: White fine-speckled black (N2)
STRUCTURE: Massive, perhaps base of sill or flow.
ALTERATION: Moderate. Plagioclase replaced by whitish and greenish clays, some with Fe-hydroxide staining. Generally greenish matrix. Whitish leucoxene associated with relict opaques. Carbonate present along grain boundaries. Short, whitish veinlets present in some areas.
VEINS/FRACTURES: 10%; 0.2-13 mm; 0-90 degrees; wide veins (0-45 orientation) and narrow veins (0-90 orientation), both infilled with carbonate and greenish clays. Veinlets often branching and cross-cutting.
ADDITIONAL COMMENTS: Generally finer grained than Sections 1 and 2 and fining steadily towards the base.

UNIT 2: SPARSELY PLAGIOCLASE-OLIVINE MICROPHYRIC BASALT

Piece 2

CONTACTS: Not actually observed. Well preserved, devitrified glassy margin in contact with veinlet at margin. Glassy rim zone grades downwards to a cryptocrystalline bottom. 45 degree inclination.
PHENOCRYSTS:
 Plagioclase - 1%; <1; Subhedral/euhedral; mostly altered to carbonate.
 Olivine - trace; <1; Subhedral/euhedral (hopper crystal morphology).
GROUNDMASS: Ranges from (a) devitrified glassy rim, (b) transition zone consisting of glass mesostasis and spherulites, (c) spherulite zone, and (d) cryptocrystalline zone with plenty of feathery and plumose variolites. Plagioclase microlites present in transition zone downwards.
VESICLES: None observed.
COLOR: Brownish gray top (5Y 5/1) to dark gray bottom (N5).
STRUCTURE: Inclined; glassy margin of a pillow or thin flow.
ALTERATION: Moderate. Plagioclase phenocrysts and microlites mostly altered to carbonate; olivine phenocrysts pseudomorphed by whitish clay. Glass is devitrified, spherulites and glass interstices altered to brown clays.
VEINS/FRACTURES: 15%; 1-80 mm; irregular; most are subparallel to glassy rim, but rest are irregular; generally branching and cross-cutting. Infilled with carbonate +/- green clays. No halos observed.
ADDITIONAL COMMENTS: Typical quenched margin to a flow.

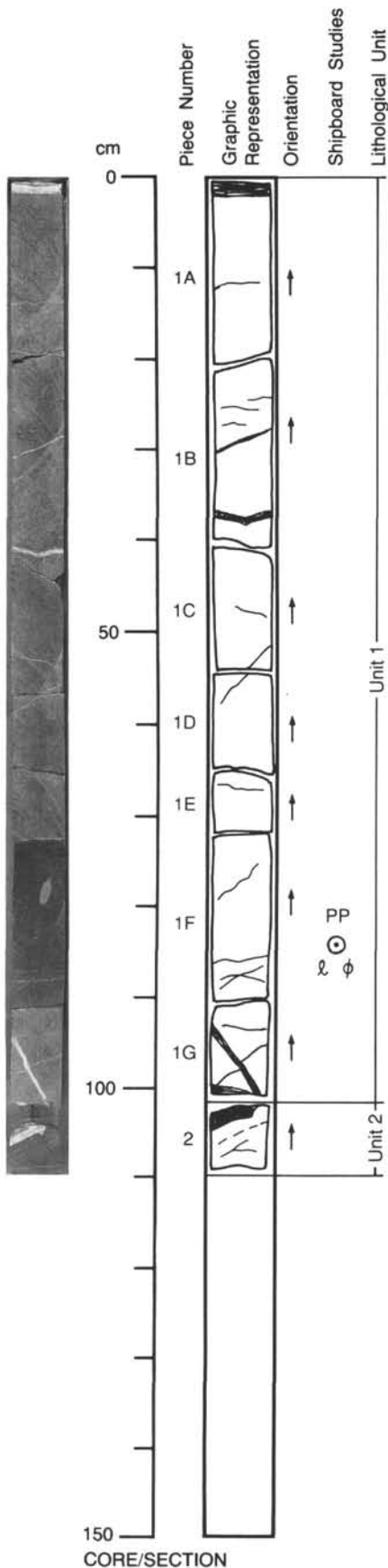


Figure 13. Example of a completed VCD form for igneous rocks.

2. A graphic representation of the core, including the rock piece numbers and positions of shipboard samples.

3. Lithologic unit boundaries, based on criteria such as the occurrence of glassy and quenched margins, trends of marked grain-size variation, and changes in petrographic type and phenocryst assemblages.

The following checklist is used for fine- and medium-grained igneous rocks. For each lithologic unit defined, note the following:

1. UNIT number (consecutive downhole), including numbers of top and bottom pieces in unit.
2. ROCK NAME (to be filled in later).
3. CONTACT TYPE. Intrusive, discordant, depositional, etc. Note the dip of the contact.
4. PHENOCRYSTS. Determine if homogeneous or heterogeneous through unit. For each phenocryst phase, list the abundance (%), average size (in mm), shape, degree of alteration (%), type and secondary phases, and any other comments.
Now fill in ROCK NAME (item 2 above.)
5. GROUNDMASS TEXTURE. Glassy, microcrystalline, fine-grained (<1 mm), medium-grained (1–5 mm). Note any relative grain-size changes within unit from piece to piece.
6. COLOR (dry).
7. VESICLES. Size, shape, percentage, distribution, and nature of any fillings. Collect similar data for miaroles (vugs).
8. STRUCTURE. Massive, pillowed, thin or sheet-like, brecciated.
9. ALTERATION. Type, form, distribution, and degree, from fresh (<2% alteration present) to slightly altered (2%–10%), moderately altered (10%–40%), highly altered (40%–80%), very highly altered (80%–95%), and completely altered (95%–100%).
10. VEINS/FRACTURES. Type, width, orientation, percent present, and nature of infillings.

Finally, any other comments may be added, including continuity of the unit within the core and interrelationship between units. When the VCD form is complete and agreed upon by the igneous petrologists, the same information is then recorded in the VAX computer database HARVI. Each record is checked by the database program for consistency and printed in a format which can be directly pasted onto the final VCD record for subsequent curatorial handling.

Igneous rocks are classified mainly on the basis of mineralogy and texture. Basalts (fine-grained) and dolerites (medium-grained) are termed aphyric if lacking phenocrysts or if they amount to <1% of the rock. If porphyritic the rock may be sparsely phyric (phenocryst content of 1%–2%), moderately phyric (2%–10%) or highly phyric (>10%). Estimates of phenocryst proportions are based on those visible with a hand lens or binocular microscope of about 10× power. Basaltic rocks may be further classified by phenocryst type: a moderately plagioclase-olivine phyric basalt contains 2%–10% total phenocrysts, most of which are plagioclase with lesser amounts of olivine.

Thin-Section Descriptions

Thin-section billets of basaltic rocks recovered during Leg 129 were examined to help define unit boundaries indicated on the VCD forms and to confirm the identity of petrographic groups and/or alteration products. At least one thin-section was made of each unit where sufficient rock was available.

Petrographic descriptions together with estimates of the various mineral phases (both primary and secondary) are

made on the igneous thin-section description forms, which are also entered up in the VAX computer database HRTHIN. Modal abundances were also determined for selected representative samples by point counting.

The mineralogical and textural effects of interaction between seawater and basement rocks was also described in thin-section, together with the nature of secondary phases infilling vesicles, fractures, and veins. Identification of secondary phases such as clays and zeolites were augmented, in some cases, by XRD.

X-ray Diffraction Analysis

A Philips ADP 3720 X-ray diffractometer was used for the XRD analysis of unknown, generally secondary mineral phases in sedimentary and igneous rocks. Instrument conditions were as follows: $\text{CuK}\alpha$ radiation with nickel filter, 40 kV, 35 mA, goniometer scan from 2° to 50° 2 θ , step size = 0.02°, count time = 2 s.

Samples were prepared by grinding in an agate pestle and mortar until reduced to a very fine powder. The resulting diffractograms were interpreted with the help of a computerized search and match routine using JCPDS powder files.

DOWNHOLE MEASUREMENTS

Tool Strings

The purpose of downhole logging is to directly determine the properties of *in-situ* formations adjacent to the borehole wall. After coring is completed in a hole, a tool string is lowered downhole on a coaxial cable, with each of several tools in the tool string continuously monitoring some property of the adjacent borehole. Of the dozens of different tool strings in common use in the petroleum industry, three Schlumberger combinations were selected for use on Leg 129: the quad combination (LSS, NGT, HLDT, and DIL), the geochemical combination (NGT, GST, and ACT), and the Schlumberger formation microscanner combination (FMS, NGT, and GPIT). In addition, the Schlumberger well seismic tool (WST) was run at Site 802. We also included the Lamont temperature tool (TLT) on the quad and geochemical combination strings. The FMS images are presented on microfiche in the back of this volume. Summary log figures appear at the end of each site chapter.

Log Types

A brief description of logging tools run during Leg 129 is given in the following section. A detailed description of logging tool principles and applications is provided in Schlumberger (1972) and Serra (1984).

Dual Induction Resistivity Log (DIL)

The DIL is a resistivity logging device that provides measurements of spontaneous potential (SP) and three resistivity values, each with a different depth of investigation: ILD (deep induction), ILM (medium induction), and SFLU (shallow, spherically focused resistivity). Because the solid constituents are orders of magnitude more resistive than the pore fluids in most rocks, resistivity is controlled mainly by the amount and connectivity of the porosity and the conductivity of the pore fluids.

Spontaneous potential is a measure of the streaming potential generated by the differences between borehole and pore-fluid electrical properties, from which both membrane and liquid junction potentials result from the differences in ion mobility in the formation and drilling fluids. The induction sonde consists of a series of transmitter coils excited by a high-frequency (25 kHz) sinusoidal current and a series of detector coils. In a nonconducting medium, the electromag-

netic field induced in the detector coils by the transmitting coils is balanced between coil pairs. In a conducting medium, the magnetic field produced by currents induced in the surrounding material induces additional currents in the receivers, changing the amplitude and phase of the total induced current. The depth of investigation is between 0.5 and 5 m, and the vertical resolution about 1.5 m.

The resistivities measured with the induction log are quite accurate for low (less than 100 ohm-m) values, but for more resistive formations it reads too low by as much as 50%–70%. In these rocks the focused resistivity log produces more reliable results. The SFLU consists of a transmitter coil and a series of focusing coils that force current into the formation laterally, away from the borehole. Without these field-shaping coils, current would tend to be conducted exclusively within the borehole. The SFLU provides a direct measurement of formation resistivity about 1 m from the well bore, with a vertical resolution of about 0.6 m.

Long-Spaced Sonic Tool (LSS)

The LSS tool is designed to measure the elastic compressional-wave velocity of the formation surrounding the borehole. In essence, the sonic tool can be thought of as a miniature seismic-refraction experiment carried out within the cylindrical borehole. A source fires acoustic energy that is transmitted into the borehole fluid. When the wavefront impinges on the borehole wall, a refracted compressional wave is generated. If the formation shear velocity is higher than the acoustic velocity of the fluid, a refracted shear wave will also be generated. The refracted waves travel along the borehole wall, reradiating energy into the fluid. Energy arrives at receivers on the logging tool at a time linearly proportional to their offset from the source. Formation elastic-wave velocities thus can be determined from the difference between the arrival times at two receivers a known distance apart.

The LSS sonde uses two acoustic transmitters spaced 2 ft apart and two receivers also spaced 2 ft apart and located 8 ft above the transmitters. This arrangement provides four source-receiver offsets of 8, 10, and 12 ft. Compensation for borehole irregularities and the inclination of the tool to the hole axis is achieved by averaging the first transit-time reading with a second reading obtained after the sonde has been raised a fixed distance along the borehole. The LSS tool records the full waveform for each source-receiver pair, in addition to automatically determining its arrival time. The LSS is centered in the borehole by the arms of a mechanical caliper (MCD) tool placed immediately above the LSS. The MCD is used only for this purpose, while borehole measurements are made with the more accurate caliper on the HLDT tool.

Compressional sonic velocity is one of the primary elastic properties measured during logging. The product of velocity and density (impedance) is useful in computing synthetic seismograms for time-depth ties of seismic reflectors.

Natural Gamma-Ray Tool (NGT)

The NGT utilizes a sodium iodide detector to determine the spectral content of naturally occurring radiation. The entire spectrum is transmitted to the surface, and the energy arriving in five preselected windows is measured by the surface electronics. The concentrations of potassium, uranium, and thorium are determined by analysis of the energy in the five bands. The spectral gamma log is commonly referred to as a KUT (K, U, and Th) log. The concentration of thorium in ppm is determined directly, whereas the concentrations of uranium in ppm and potassium in wt% are determined by a stripping technique.

The relative proportions of K, Th, and U are controlled by the mineralogy, clay content, and alteration history. Clay type is determined from the relative abundances of thorium and potassium, the primary radioactive elements in clay. Uranium is commonly associated with organic matter in carbonates. The vertical resolution of the tool is about 0.25 m.

Lithodensity Tool (HLDT)

The HLDT contains a chemical source (^{137}Ce) of 0.66-MeV gamma rays. The two detectors measure the flux of transmitted gamma rays in a series of energy windows to determine density (RHOB) and photoelectric factor (PEF). A measure of tool performance based on the energy distribution at the near and far receivers (DRHO) is also provided. Gamma rays with energies less than 1.01 MeV interact with atoms in the formation by Compton scattering and via the photoelectric effect. Compton scattering is an elastic collision by which energy is transferred between the gamma ray and electron in the formation. This interaction forms the basis of the density measurement. In effect, the HLDT measures electron density directly, and formation density is determined using the fact that the atomic weight is approximately twice the atomic number in most rock-forming elements. At low energies (below about 0.06 MeV) gamma rays are subject to absorption via the photoelectric effect. One of the energy windows on the far detector is tuned to measure this effect, and the measurement is inverted to obtain the PEF determination. Because this measurement is almost independent of porosity it can be used directly as a matrix lithology indicator.

The depth of investigation of the lithodensity tool depends on the density of the rock: the higher the density, the lower the penetration. In porous and permeable formations the density tool does not read deeper than 0.16 m. The vertical resolution is about 0.3 m. The caliper arms on the HLDT that force the tool against the borehole wall are also used to measure borehole size. These measurements are primarily used to indicate bad parts of the hole, where other logs may read inaccurately, and to correct the responses of those logs sensitive to less severe variations in hole size. The caliper response can also be indicative of lithology. For instance, in zones with swelling clays, hole constrictions are observed where the caliper reads less than the bit size. In addition, as hole conditions in general are a consequence of rock properties, variations in hole size may correlate with lithologic changes.

Gamma Spectrometry Tool (GST)

The GST consists of a pulsed source of 14-MeV neutrons and a gamma-ray scintillation detector. A surface computer performs spectral analysis of gamma rays resulting from the interactions of neutrons emitted by the source with atomic nuclei in the formation. Characteristic sets of gamma rays from six elements dominate the spectrum, permitting calculation of six elemental yields: calcium, silica, iron, chlorine, hydrogen, and sulfur. As the normalized sum of their abundance is always one, values do not reflect the actual elemental composition. Instead, ratios of these yields are commonly used in interpreting the lithology, porosity, and salinity of the formation fluid.

Aluminum Clay Tool (ACT)

Aluminum abundance as measured by the ACT is determined by neutron-induced (cf. chemical source) late gamma-ray spectrometry. By placing sodium iodide detectors both above and below the neutron source, contributions from natural gamma-ray activity can be removed. Calibration to elemental wt% is performed by taking irradiated core samples of known volume and density and measuring their gamma-ray

output while placed in a jig attached to the logging tool (generally after logging).

General Purpose Inclinator Tool (GPIT)

This tool determines the hole azimuth and deviation and the vector components of the magnetic field. Although it is not oriented gyroscopically, the GPIT can accurately measure the magnetic field inclination. The device also monitors vertical and horizontal accelerations applied to the logging probe and thus can be used to determine the effects of ship heave on the logging run.

Lamont Temperature Tool (TLT)

The TLT is self-contained and can be attached to any of the sensor combinations. Data from two thermistors and a pressure transducer are collected every 0.5–5.0 s and stored within the tool. Once the *in-situ* measurement is completed the data are transferred to a shipboard computer for analysis. The fast-response thermistor, though low in accuracy, is able to detect small abrupt temperature excursions caused by fluid flow from the formation. The slow-response thermistor has a high accuracy and can be used to estimate the temperature gradient. Data are recorded as a function of time, with conversion to depth based on the pressure transducer (or preferably, based on simultaneous recording by Schlumberger of both depth and time).

Formation Microscanner Tool (FMS)

The formation microscanner produces high-resolution borehole images from electrical conductivity measurements (Ekstrom et al., 1986; Pezard and Luthi, 1988). Its application as used in the petroleum oil industry since 1986 has been precluded in ODP because of constraints imposed by the internal diameter (4.125 in.³) of the drill pipe. A modified sensor was consequently developed by Schlumberger for ODP and first deployed during Leg 126. The FMS has a vertical resolution of approximately 1 cm, but a detection threshold for conductive features of the order of microns. This fine-scale detection ability (raw data points are recorded every 2.5 mm) allows for the detailed study of subsurface structures.

In contrast, typical conventional downhole measurements are averaged over 150 mm; thus the sampling rate of the FMS is 60 times larger than most other logging devices. The FMS has four orthogonal pads which are pressed against the borehole wall. In the original version developed by Schlumberger, two adjacent pads each carry an array of 27 closely spaced electrodes, from which two electrical images are derived. The electrode currents probe the conductivity of the rock to a depth of a few cm into the borehole wall, responding to variations in physical and chemical properties of the rock such as porosity and surface conduction. The series of conductivity traces are displayed side-by-side and coded into an image in which black represents the most conductive values and white the most resistive ones. The new ODP sensor was designed in such a way that four images of 16 traces each are recorded simultaneously. In addition, the resolution of the images is improved due to the smaller size of the electrode array.

Once the data have been acquired in the borehole, the images are processed on a devoted workstation to allow for on-site comparison with the cores. In the future, a graphic analysis software will be installed on the ship using a Macintosh II color workstation in order to perform such basic analysis as the interactive mapping of geological features. Possible applications of the FMS-derived images include: detailed correlation of coring and logging depths, orientation of cores, mapping of fractures, faults, foliations, and forma-

tion structures, and the analysis of depositional environments (with information on transport direction, structure of the pore space, nature of contacts, and depositional sequences). The formation microscanner also provides precise measurements of borehole diameter in two orthogonal directions. In an isotropic, linearly elastic rock subjected to an anisotropic stress field, breakouts form along the borehole wall as a result of compressive stress concentrations exceeding the strength of the rock. Under these conditions, the breakout orientation develops in the direction of the least principal horizontal stress. It has been previously demonstrated that stress orientations deduced from rock breakouts are consistent with other independent indicators (Bell and Gough, 1979; Zoback et al., 1988).

Well Seismic Tool (WST)

Vertical seismic profiles are typically run with a surface sound source and receivers (geophones) such as the WST down the hole. At each receiver location, multiple shots are taken to allow stacking for noise reduction. During Leg 129 at Site 802, several problems were encountered with both the tool and the surface equipment, permitting only several shots to be recorded.

Log Analysis

During logging, incoming data were observed in real time on a monitor oscilloscope and simultaneously recorded on digital tape in the Schlumberger logging unit. After logging, this tape was copied from 800 to 1600 bpi on the shipboard VAX computer system. The 1600 bpi tape was then read by the Masscomp computer system in the downhole logging laboratory aboard ship and reformatted to a FLIC format compatible with the "Terralog" log-interpretation software package. Rather than being a "black box," Terralog is an interactive system consisting of many log manipulation and plot options. Thus, the log analysis and interpretation varied in duration and procedure for each site. Log display and preliminary interpretation were carried out aboard ship; further analysis and interpretation were undertaken after the cruise, using a companion system in the Borehole Research Laboratory of Lamont-Doherty Geological Observatory. Logs are presented at the end of individual site chapters in a series of summary diagrams.

SITE GEOPHYSICS AND SEISMIC STRATIGRAPHY

Site selection for Leg 129 was based on the multichannel seismic (MCS) surveys conducted aboard the *Fred H. Moore* during the FM35-12 expedition (November-December 1987) and aboard *Le Suroit* during the MESOPAC II expedition (August-September 1989). Underway geophysical data were collected as we approached all sites and provided the correlations with principal MCS sections needed to position the ship at preferred locations. Instrumentation on board included precision echo-sounders, a magnetometer, a seismic reflection acquisition system, and satellite navigation systems.

Navigation

Navigation data were collected on the bridge and in the underway geophysics laboratory using a Magnavox MX1107 satellite navigation system (SATNAV), which accesses both transit and global positioning system (GPS) satellites. Positions were recorded on magnetic tape and paper records every 2 min during non-seismic transits and every 14 s (i.e., every shotpoint) during seismic operations. Routine collection of navigation data includes recording course and speed data by HIGHRES, the shipboard seismic data acquisition software

package. The more accurate GPS fixes were available for 12 to 14 hr each day when at least three satellites were accessible.

When possible, site approach surveys were carried out during times of GPS coverage (see "Operations" sections in each site chapter for details). The final site locations are an average of all SATNAV positions collected while on location. The ship's track for Leg 129 was generated from satellite navigation course and speed information using the SMOOTH program aboard the *JOIDES Resolution*.

Bathymetry

Bathymetric data were recorded with both 3.5- and 12-kHz echo-sounder systems. The signals were displayed on two Raytheon recorders with 1-s sweeps (750 m/sweep). The quality of these records was quite poor during the full speed (9 kt) transit from Guam, principally due to ship motion and noise as we headed northeast into 25 kt winds and the resulting rough seas. However, during our final approach to Site 800 and subsequent Sites 801 and 802, at approximately 6.5 kt the 3.5-kHz system provided excellent records that assisted in site location. During subsequent full-speed transits (between Sites 800 and 801, and Sites 801 and 802) these echo-sounder systems provided good quality records.

Magnetics

Total intensity measurements of the Earth's magnetic field were obtained with a Geometrics 801 proton precession magnetometer towed approximately 400 m astern. The data were recorded continuously on a graphic recorder and in the header record of seismic tapes, once per shot. The magnetometer was not operational during the first few days of the cruise, but was operational during the approach to all three site locations and intervening transits.

Seismic Reflection Acquisition and Processing

Single-channel seismic reflection (SCS) data collected during the final approach to all site locations were recorded using the following equipment and parameters. The seismic source consisted of two synchronized 80-in.³ water guns operating at 1900 psi at a repetition rate of 14 s. The guns were towed approximately 25 m behind the ship and 14 m apart. Reflections were recorded with a teledyne "high speed" streamer with a 100-m-long active section containing 60 hydrophones, a 15-m-long "stretch" section, and a 488-m lead section. The head of the streamer was positioned approximately 503 m behind the ship. The water guns and streamer were towed at estimated depths of 7–8 m and 10–12 m, respectively. Raw data were filtered (25–250 Hz) and recorded with a 6- or 7-s delay for 5 s on 1600 bpi magnetic tape in SEG Y format, at a 1-msec sampling interval. The one exception to this occurred during the approach to Site 801 when an error in setting the deep-water delay resulted in inadequate data coverage (only .5 s two-way traveltimes below seafloor were recorded). This problem was rectified and a short post-site survey successfully obtained adequate SCS coverage across Site 801. Upon playback of the digital SCS record across Site 801, another acquisition problem was recognized; all the data appeared to be clipped. The most likely explanation for this is that the input gain was set too high, so that the system digitizer was overdriven with voltages in excess of 5 V. The streamer signal was also passed through amplifiers and band-pass filters (20–150 Hz, 30–150 Hz) for real-time display on two EDO 550 dry-paper analog recorders set with a 4 s sweep.

The seismic system employs a super-micro 561 Masscomp computer to record, process, and display data. Although time-consuming, the shipboard processing package (SI-OSEIS) proved useful in providing large-scale plots of win-

dowed data for interpretation, including comparisons with synthetic seismograms derived from logging data (see "Down-hole Measurements" sections, "Site 800" and "Site 802" chapters, this volume).

Site Surveys

The FM35-12 expedition collected over 3900 km of MCS data using a 2819-in.³ air-gun array seismic source and a 3.3-km-long, 96-channel receiving streamer (Abrams et al., 1988). Refraction data collected by seven long-range sonobuoys were also digitally recorded during this regional survey. The MESOPAC II MCS survey focused on potential drilling targets first identified on FM35-12, as well as investigated the northern Pigafetta Basin within the oldest portion of the M-sequence lineation pattern. The MESOPAC II expedition also recorded approximately 3900 km of MCS data using six 80-in.³ water guns during vertical incident profiling and two 1000-in.³ air guns while digitally recording refraction data from six long-range sonobuoys. Seismic signals were received by a 2.7-km-long, 96-channel streamer. The MESOPAC II expedition also acquired high quality 3.5-kHz records used as a final constraint on site location. The MCS vertical incidence data recorded with both large volume air-gun and water-gun sources, along with refraction data from long-range sonobuoys, provided the best possible constraints for locating potential drill sites.

Sonobuoy Analysis

In an effort to further define the seismic structure of the East Mariana and Pigafetta basins, we have analyzed reflection and refraction data collected simultaneously with MCS using long-range sonobuoys. The combination of vertical incidence MCS data and wide angle reflection/refraction data from sonobuoys provide the best possible estimate of sub-bottom structure (short of drilling) in these two basins. Major emphases in this area of the Pacific, where oceanic crust is unusually smooth and/or overlain by draping diagenetic or volcanic intrusive horizons, are the identification of a crust/sediment interface and, secondarily, determination of crustal velocity structure.

The sonobuoy T/X data from both FM35-12 and MESOPAC II were inverted to a layered isovelocity vs. depth model using the tau- p method of Diebold and Stoffa (1981). At the time of Leg 129, only analog records of the MESOPAC II sonobuoys were available; the following processing and analyses involving digital manipulation apply only to FM35-12 sonobuoys. The isovelocity model was used as a starting point for interactive one-dimensional ray tracing, which allowed for vertical velocity gradients and iterative real-time comparison of modeled vs. observed T/X data. Absolute amplitudes were not modeled, but relative amplitudes were used to qualitatively access velocity gradients and to locate critical points on mantle arrivals. The primary limitations of this modeling are (1) the assumption of one-dimensionality and (2) the non-uniqueness of any "best fit" model, particularly the inherent ambiguity between variations in layer thickness and velocity in modeling traveltimes. The assumption of one-dimensionality appears justified in this area where the seafloor is essentially flat (± 15 m) over the 40- to 50-km range of these buoys, and except for FM35-12 sonobuoy 23, the highest amplitude sub-bottom reflections are also flat-lying ($<10^\circ$ dip). There are some buoys, however, that are disturbed by out-of-plane effects. Direct wave arrivals were used to calculate ranges assuming a D-wave channel velocity of 1.54 km/s estimated from CTD measurements made during the FM35-12 cruise. Changes in the D-wave slope, indicating a change in distance/shot (assuming constant V_w), were apparent on some

sonobuoy records; and these variations in range were included in our modeling. Sonobuoy data were not used to derive sediment velocities (i.e., velocities between the seafloor and the first refraction). Sediment velocities were based on velocity analysis of four contiguous CDP gathers from the 3.3 km-long, 96-channel streamer. Sediment velocities derived from MCS velocity analysis ranged from 1.6 to 3.0 km/s, usually increasing with depth. This range in velocities is similar to velocities derived from T2/X2 sonobuoy solutions in the northwest Pacific and those measured during DSDP Legs 20, 32, and 89 (Heezen, MacGregor, et al., 1973; Larson, Moberly, et al., 1975; Moberly, Schlanger, et al., 1986). Only one or two of the highest amplitude reflectors were matched by velocity contrasts in the model, and sediments were divided into isovelocity layers even though it is recognized that velocity gradients may also occur.

The depth to the crust/sediment interface depends on the overlying velocity structure and was chosen based on the depth to the first refracted arrivals. Often precritical refracted arrivals were observed within the near vertical reflections and traced to their tangency to a sub-bottom reflection. These continuously curved refractions are indicative of velocity gradients. Wide angle reflection events from the Moho were also modeled; the curvature of these events was constrained by the overlying velocity structure, whereas the underlying mantle velocity was constrained by our choice of critical point location. The slope of a line drawn tangent to this reflection can also give an estimate of mantle velocity.

REFERENCES

- Abrams, L. J., Larson, R. L., Shipley, T., and Lancelot, Y., 1988. Cretaceous volcanic sequences and Jurassic(?) crust in the western Pacific, *Trans. Am. Geophys. Union*, 69:1442.
- Baumgartner, P. O., 1984. A Middle Jurassic–Early Cretaceous low-latitude radiolarian zonation based on Unitary Associations and age of Tethyan radiolarites. *Eclogae Geol. Helv.*, 77(3):729–837.
- , 1987. Age and genesis of Tethyan Jurassic Radiolarite. *Eclogae Geol. Helv.*, 80(3):831–879.
- Bell, J. S., and Gough, D. I., 1979. Northeast-southwest compressive stress in Alberta: evidence from oil wells, *Earth Planet. Sci. Lett.*, 45:475–482.
- Berggren, W. A., and Miller, K. G., 1988. Paleogene tropical planktonic foraminiferal biostratigraphy and magnetobiochronology. *Micropaleontology*, 34(4):362–380.
- Berggren, W. A., Kent, D. V., and Flynn, J. J., 1985a. Paleogene geochronology and chronostratigraphy. In Snelling, N. J. (Ed.), *Geochronology and the Geologic Time Scale*: Geol. Soc. London Mem., 10:141–195.
- Berggren, W. A., Kent, D. V., and van Couvering, J. A., 1985b. Neogene geochronology and chronostratigraphy. In Snelling, N. J. (Ed.), *Geochronology and the Geologic Time Scale*: Geol. Soc. London Mem., 10:211–260.
- Blow, W. H., 1969. Late middle Eocene to Recent planktonic foraminiferal biostratigraphy. In Brönnimann, P., and Renz, H. H. (Eds.), *Proc. 1st Intl. Conf. Planktonic Microfossils*: Leiden (E. J. Brill), 199–241.
- Bolli, H. M., and Saunders, J. B., 1985. Oligocene to Holocene low latitude planktic foraminifera. In Bolli, H. M., Saunders, J. B., and Perch-Nielsen, K. (Eds.), *Plankton Stratigraphy*: Cambridge (Cambridge Univ. Press), 155–262.
- Boyce, R. E., 1976. Definitions and laboratory determination of compressional sound velocity parameters and wet-water content, wet-bulk density and porosity parameters by gravimetric and gamma-ray attenuation techniques. In Schlanger, S. O., Jackson, E. D., et al., *Init. Repts. DSDP*, 33: Washington (U.S. Govt. Printing Office), 931–958.
- Bralower, T. J., 1987. Valanginian to Aptian calcareous nannofossil stratigraphy and correlation with the upper M-sequence magnetic anomalies. *Mar. Micropaleont.*, 11:293–310.
- Bralower, T. J., Monechi, S., and Thierstein, H. R., 1989. Calcareous nannofossil zonation of the Jurassic-Cretaceous boundary interval and correlation with the geomagnetic polarity timescale. *Mar. Micropaleont.*, 14:153–235.
- Bukry, D., 1973. Low-latitude coccolith biostratigraphic zonation. In Edgar, N. T., Saunders, J. B., et al., *Init. Repts. DSDP*, 15: Washington (U.S. Govt. Printing Office), 685–703.
- , 1975. Coccolith and silicoflagellate stratigraphy, northwestern Pacific Ocean, Deep Sea Drilling Project, Leg 32. In Larson, R. L., Moberly, R., et al., *Init. Repts. DSDP*, 32: Washington (U.S. Govt. Printing Office), 677–701.
- Carlson, R. L., and Christensen, N. L., 1979. Velocity anisotropy in semi-indurated calcareous deep-sea sediments. *J. Geophys. Res.*, 84:205–211.
- Caron, M., 1985. Cretaceous planktic foraminifera. In Bolli, H. M., Saunders, J. B., and Perch-Nielsen, K. (Eds.), *Plankton Stratigraphy*: Cambridge (Cambridge Univ. Press), 17–86.
- Diebold, J., and Stoffa, P., 1981. The travelttime equation, tau-p mapping, and inversion of common-midpoint data, *Geophysics*, 46:238–254.
- Ekstrom, M. P., Dahan, C. A., Chen, M. Y., Lloyd, P. M., and Rossi, D. J., 1986. Formation imaging with microelectrical scanning arrays. *Trans. 27th Ann. Logging Symp., Soc. of Prof. Well Log Analysts*, Paper BB.
- Fischer, R. V. and Schminke H. V., 1984. *Pyroclastic Rocks*: Berlin (Springer-Verlag).
- Gealy, E. L., Winterer, E. L., and Moberly, R., 1971. Methods, conventions, and general observation. In Winterer, E. L., Riedel, W. R., et al., *Init. Repts. DSDP*, 7: Washington (U.S. Govt. Printing Office), 9–26.
- Gieskes, J. M. and Peretsman, G., 1986. Water chemistry procedures aboard JOIDES Resolution: Some comments. *ODP Tech. Note*, 5.
- Hamilton, E. L., 1971. Prediction of *in-situ* acoustic and elastic properties of marine sediments. *Geophysics*, 36:266–284.
- Hay, W. W., Sibuet, J.-C., et al., 1984. Introduction and explanatory notes, Deep Sea Drilling Project Leg 75. In Hay, W. W., Sibuet, J.-C., et al., *Init. Repts. DSDP*, 75 (Pt. 1): Washington (U.S. Govt. Printing Office), 3–25.
- Hedberg, H. D., 1976. *International Stratigraphic Guide*: New York (Wiley, New York).
- Heezen, B. C., MacGregor, I. D., et al., 1973. *Init. Repts. DSDP*, 20: Washington (U.S. Govt. Printing Office).
- Isaacs, C. M., 1982. Influence of rock composition on kinetics of silica phase changes in the Monterey Formation, Santa Barbara area, California. *Geology*, 10:304–308.
- Kent, D. V., and Gradstein, F. M., 1985. A Cretaceous and Jurassic geochronology. *Geol. Soc. Am. Bull.*, 96:1419–1427.
- Larson, R. L., Moberly, R., et al., 1975. *Init. Repts. DSDP*, 32: Washington (U.S. Govt. Printing Office).
- Manheim, F. T., and Sayles, F. L., 1974. Composition and origin of interstitial water of marine sediments based on deep sea drilled cores. In Goldberg, E. D. (Ed.), *The Sea* (Vol. 5): New York (Wiley Interscience), 527–568.
- Martini, E., 1971. Standard Tertiary and Quaternary calcareous nannoplankton zonation. In Farinacci, A. (Ed.), *Proc. 2nd Planktonic Conf.*, Rome (Ed. Tecnoscienza), 739–785.
- Matsuoka, A., and Yao, S., 1985. Latest Jurassic radiolarians from the Torinosu Group in Southwest Japan. *J. Geosci., Osaka City Univ.*, 28:125–145.
- , 1986. A newly proposed radiolarian zonation for the Jurassic of Japan. *Mar. Micropaleont.*, 11:91–106.
- Moberly, R., Schlanger, S. O. et al., 1986. *Init. Repts. DSDP*, 89: Washington (U.S. Govt. Printing Office).
- Monechi, S., and Thierstein, H. R., 1985. Late Cretaceous-Eocene nannofossil and magnetostratigraphy correlations near Gubbio, Italy. *Mar. Micropaleont.*, 9:419–440.
- Ogg, J. G., 1987. Early Cretaceous and Tithonian magnetostratigraphy of the Galicia margin (Ocean Drilling Program Leg 103). In Boillot, G., Winterer, E. L., et al., *Proc. ODP, Sci. Results*, 103: College Station, TX (Ocean Drilling Program), 659–682.
- Okada, H., and Bukry, D., 1980. Supplementary modification and introduction of code numbers to the low-latitude coccolith biostratigraphic zonation (Bukry, 1973; 1975). *Mar. Micropaleont.*, 5:321–325.

- Pezard, P. A., and Luthi, S. M., 1988. Borehole electrical images in the basement of the Cajon Pass scientific drill hole, California: fracture identification and tectonic implications. *Geophys. Res. Lett.*, 15:1017-1020.
- Ratcliffe, E. H., 1960. The thermal conductivities of ocean sediments. *J. Geophys. Res.*, 65:1535-1541.
- Riedel, W. R., and Sanfilippo, A., 1978. Stratigraphy and evolution of tropical Cenozoic radiolarians. *Micropaleontology*, 24:61-96.
- Roth, P. H., 1978. Cretaceous nannoplankton biostratigraphy and oceanography of the northwestern Atlantic Ocean. In Benson, W. E., Sheridan, R. E., et al., *Init. Repts. DSDP*, 44: Washington (U.S. Govt. Printing Office), 731-759.
- _____, 1983. Jurassic and Lower Cretaceous calcareous nanofossils in the Western North Atlantic (Site 534): Biostratigraphy, preservation, and some observations on biogeography and paleoceanography. In Sheridan, R. E., Gradstein, F. M., et al., *Init. Repts. DSDP*, 76: Washington (U.S. Govt. Printing Office), 587-621.
- Sanfilippo, A., and Riedel, W. R., 1985. Cretaceous radiolaria. In Bolli, H. M., Saunders, J. B., and Perch-Nielsen, K. (Eds.), *Plankton Stratigraphy*: Cambridge (Cambridge Univ. Press), 573-630.
- Sanfilippo, A., Westberg-Smith, M. J., and Riedel, W. R., 1985. Cenozoic radiolaria. In Bolli, H. M., Saunders, J. B., and Perch-Nielsen, K. (Eds.), *Plankton Stratigraphy*: Cambridge (Cambridge Univ. Press), 631-712.
- Schlumberger, Inc., 1972. *Log Interpretation* (Vol. 1): New York (Schlumberger).
- Schmid, R., 1981. Descriptive nomenclature and clarification of pyroclastic deposits and fragments: recommendations of the IUGS Subcommittee on the Systematics of Igneous Rocks. *Geology*, 9:41-43.
- Serra, O., 1984. *Fundamentals of Well Log Interpretation*: Amsterdam (Elsevier).
- Shepard, F. P., 1954. Nomenclature based on sand-silt-clay ratios. *J. Sediment. Petrol.*, 24:151-158.
- Shipboard Scientific Party, 1989. Introduction and explanatory notes. In Robinson, P. T., Von Herzen, R., et al., *Proc. ODP, Init. Repts.*, 118: College Station, TX (Ocean Drilling Program).
- Sissingh, W., 1977. Biostratigraphy of Cretaceous calcareous nannoplankton. *Geol. Mijnbouw*, 56(1):37-65.
- Steiner, M. B., and Ogg, J. G., 1988. Early and Middle Jurassic magnetic polarity time scale. In Rocha, B. (Ed.), *Proc. 2nd Int. Jurassic Stratigraphy Symp.*, Lisbon, Sept. 14-18, 1987 (Geol. Surv. Denmark).
- Supko, P., Ross, D. A., and Neprochnov, Y. P., 1978. Introduction and explanatory notes, Leg 42B, Deep Sea Drilling Project. In Ross, D. A., Neprochnov, Y., P., et al., *Init. Repts. DSDP*, 42, Pt. 2: Washington (U.S. Govt. Printing Office), 3-15.
- Thierstein, H. R., 1976. Mesozoic calcareous nannoplankton biostratigraphy of marine sediments. *Mar. Micropaleont.*, 1:325-362.
- _____, 1973. Lower Cretaceous calcareous nannoplankton biostratigraphy. *Abh. Geol. Bundesanst. (Austria)*, 29:1-52.
- _____, 1971. Tentative Lower Cretaceous nannoplankton zonation. *Eclogae Geol. Helv.*, 64:459-488.
- Toumarkine, M., and Luterbacher, H., 1985. Paleocene and Eocene planktic foraminifera. In Bolli, H. M., Saunders, J. B., and Perch-Nielsen, K. (Eds.), *Plankton Stratigraphy*: Cambridge (Cambridge Univ. Press), 87-154.
- Vaquier, V., 1985. The measurement of thermal conductivity of solids with a transient linear heat source on the plane surface of a poorly conducting body. *Earth Planet. Sci. Lett.*, 74:275-279.
- Von Herzen, R. P., and Maxwell, A. E., 1959. The measurements of thermal conductivity of deep-sea sediments by a needle probe method. *J. Geophys. Res.*, 64:1557-1563.
- Wentworth, C. K., 1922. A scale of grade and class terms of clastic sediments. *J. Geol.*, 30:377-390.
- Williams, G. L., 1977. Dinocysts: their paleontology, biostratigraphy and paleoecology. In Ramsay, A.T.S. (Ed.), *Oceanic Micropaleontology*, 2:1231-1325.
- Zoback, M. D., Zoback, M. L., Mount, V. S., Suppe, J., Eaton, J. P., Healy, J. H., Oppenheimer, D., Reasenber, P., Jones, L., Raleigh, C. B., Wong, I. G., Scotti, O., and Wentworth, C., 1988. New evidence on the state of stress of the San Andreas Fault, *Science*, 238:1105-1111.

Ms 129A-101